Diplomarbeit

Ginzburg-Landau approach to the QCD phase diagram

Ausgeführt am Institut für

Theoretische Physik

der Technischen Universität Wien

bei

Univ.-Prof. DI Dr. Anton Rebhan

unter Anleitung von

Univ.Ass. Dr. Andreas Schmitt

durch

Stephan Stetina

Wien, 24.11.2010

Müsset im Naturbetrachten

Immer eins wie alles achten;

Nichts ist drinnen, nichts ist draußen;

Denn was innen, das ist außen.

So ergreifet, ohne Säumnis,

Heilig öffentlich Geheimnis.

Goethe

Introduction and motivation

High-energy physics , elementary particle physics and the theory of fundamental interactions have always been my strongest motivation to study physics. Some of the probably most fascinating questions of modern physics lie within these disciplines. Here are just a view examples: What was the state of matter in our universe shortly after the "Big-Bang"? What happened in the cooling process of the universe, leading to the physical environment we experience today? What happens to matter within incredibly dense astrophysical objects such as neutron stars? Of course, I am not going to address all these questions in detail , but many of these aspects are closely related to the study of the QCD phase diagram, which is at the center of this work. Practically all of the above questions can at least partially be answered through the very powerful and intriguing concept of symmetries and a big part of this work will be devoted to their discussion.

Another strong motivation to participate in research in this specific area is given by its interdisciplinarity. Despite obvious relations to astrophysics and nuclear physics we also find marked similarities to solid-state physics. Most of the concepts used in the frame of this work, such as superconductivity or spontaneous symmetry breaking even originate from solid-state physics. Finally, the key tool for the subsiding analysis of the QCD phase diagram, the Ginzburg-Landau formalism was also primarily developed in order to study typical quantities of solid state physics, such as magnetism or superconductivity of electrons. Additionally, we require other theoretical tools such as statistical physics, or quantum-field theories, which underlines the diversity of this field of studies. The Ginzburg-Landau formalism by itself has proved to be quite pedagogical and instructive. All key features of the theory one wants to model have to be introduced to the Ginzburg-Landau potential manually which is probably the most effective way to understand the physical properties of a system.

At this point, I would like to express my deepest gratitude to my supervisor Andreas Schmitt, who invested a considerable amount of time in answering my questions, dissolving misunderstandings and providing ideas on how to solve upcoming problems. This way, I have learned a great deal not only about technical details within certain calculations, but also about how to decompose a project into small steps and how to apply reasonable simplifications to otherwise insuperable problems.

This work was carried out in cooperation with Andreas Schmitt (TU Vienna) and Motoi Tachibana (Saga University). The main results have also been summarized in a paper which has been submitted to Phys. Rev. D (arXiv:1010.4243 [hep-ph]).

Contents

Chapter 1

Physical foundations

As indicated in the introduction, the study of the phase structure of strong interacting matter requires a large variety of theoretical tools. The aim of this chapter is to provide a short introduction to some of them. We begin by summarizing the most basic facts about Quantum Chromodynamics and thermal field theories. However, our main focus are non perturbative concepts, such as chiral symmetry breaking we will discuss them in some more detail. Special emphasis will be placed on symmetries and their breaking patterns. Then, we discuss the ground state of high density quark matter as well as meson condensation in such a high density system. At the end, we introduce the (speculative) phase diagram of Quantum Chromodynamics, which embodies most of the physics discussed in this chapter. However, the most important tool for this work, the Ginzburg-Landau formalism, will be discussed in the beginning of chapter 2.

1.1 Quantum Chromodynamics (QCD) in a nutshell

In this section, we quickly review the most basic properties of QCD which is an $SU(3)_{color}$ gauge theory of strong interactions, embedded in the full symmetry group of the standard-model of particle physics $G = U(1)_{em} \otimes SU(2)_{weak} \otimes SU(3)_{color}$. The charges of the interacting particles (quarks) are given by the colors red, green and blue, the interactions are mediated by (8) Gluons. The corresponding QCD-Lagrangian is given by:

$$\mathcal{L}_{QCD} = -\frac{1}{2} G_{\mu\nu} G^{\mu\nu} + \bar{\Psi}(i\gamma^{\mu} D_{\mu} - M)\Psi \tag{1}$$

The field strengths are expressed by $G_{\mu\nu} = \partial_{\mu} A_{\nu} - \partial_{\nu} A_{\mu} - ig[A_{\mu}, A_{\nu}]$ and the covariant derivative by $D_{\mu} = \partial_{\mu} - igA_{\mu}$. g denotes the strong coupling constant, and A_{μ} are matrices in the Lie Algebra of the gauge group of $SU(N_C)$. Dirac indices are denoted by μ and ν. Since in QCD, the number of colors $N_C = 3$, $SU(3)_C$ denotes the group of unitary $N_C \otimes N_C$=3 $\otimes$ 3 matrices with determinant 1 and dimension $Dim[SU(3)] = 3^2 - 1 = 8$. We hence require 8 generators which fulfill the following relations:

$$[T_a, T_b] = i f_{abc} T_c, \qquad T_a^{+} = T_a, \qquad \mathrm{Tr}[T_a T_b] = \frac{1}{2}\delta_{ab}, \qquad T_a = \frac{\lambda_a}{2} \tag{2}$$

The matrices λ_a are given by the Gell-Mann matrices. We can now decompose the Gauge(Gluon) fields and field strenghts into:

$$A_{\mu} = A_{\mu}^{a} T_a, \qquad G_{\mu\nu} = G_{\mu\nu}^{a} T_a, \qquad G_{\mu\nu}^{a} = \partial_{\mu} A_{\nu}^{a} - \partial_{\nu} A_{\mu}^{a} + g f^{abc} A_{\mu}^{b} A_{\nu}^{c} \tag{3}$$

Additionally to introducing the gauge symmetry of $SU(3)_C$, which is an exact symmetry of the QCD Lagrangian, we also need to take into account different quark flavors (up,down and strange). However, the corresponding symmetry of $SU(N_f)$ is only approximately fulfilled for up down quarks, whereas the strange quark is much heavier:

flavor	mass $[\frac{MeV}{c^2}]$
u	1.5...4.5
d	2.5...5.5
s	80...155
c	1.0...1.4 $\cdot 10^3$
b	4.0...4.4$\cdot 10^3$
t	189.8...188.5$\cdot 10^3$

Table1: Quark masses according to the Particle Data Book (PDB).

Flavor symmetries are of fundamental interest for our work, and we will discuss them in some detail in section 1.3. The explicit expression of the Lagrangian including fundamental color indices α,β , ad-joint color index a and flavor indices i, j is then given by:

$$\mathcal{L}_{QCD} = -\frac{1}{2}G^a_{\mu\nu}G^{\mu\nu}_a + \bar{\Psi}^\alpha_i[i\gamma^\mu(\delta^{\alpha\beta}\partial_\mu - igA^a_\mu T^{\alpha\beta}_a) - \delta^{\alpha\beta}m_i]\Psi^\beta_j \tag{4}$$

From this Lagrangian, we can construct quark and gluon 2-point functions (propagators) as well as quark-gluon and gluon-gluon vertices. Applying the path integral formalism, we can perform perturbative calculations using the generating functional,

$$\left\langle 0 \left| TA^\alpha_\mu(....)A^\beta_\nu\Psi(.....)\bar{\Psi}\right| 0\right\rangle = \frac{\int D[A\Psi\bar{\Psi}\eta\eta^*]A^\alpha_\mu(....)A^\beta_\nu\Psi(.....)\bar{\Psi}\sum_N \frac{(iS_I)^N}{N!}\exp(iS_0)}{\int D[A\Psi\bar{\Psi}\eta\eta^*]\sum_N \frac{(iS_I)^N}{N!}\exp(iS_0)} \tag{5}$$

which also contains the ghost\anti-ghost contributions η and η^* as a consequence of gauge fixing. Hence, the full QCD Lagrangian is of the form $\mathcal{L} = \mathcal{L}_{QCD} + \mathcal{L}_{gauge-fix} + \mathcal{L}_{ghost}$ and the corresponding action can be divided in interacting and non-interacting parts which are denoted by S_0 and S_I in the above formula. The interacting part now also contains additional gauge-ghost interactions. However, since we are not going to perform perturbative QCD calculations in the frame of this work, we are not going to work out any more explicit details. For our consideration much more interesting are non-perturbative effects in QCD which we shall discuss in section 1.4.

1.2 QCD at finite temperature T and chemical potential μ

We will now give a brief introduction to the basics tools of QCD at finite T and μ, which we require for our subsequent analysis of the phase diagram. The proper way to introduce a quark chemical potential into the QCD Lagrangian is by treating it like a temporal component of a gauge field that couples to fermions:

$$\mathcal{L}_{QCD} = -\frac{1}{2}G_{\mu\nu}G^{\mu\nu} + \bar{\Psi}(i\gamma^\mu D_\mu + \gamma^0\mu - m)\Psi \tag{6}$$

However, we are not going to use the full QCD Lagrangian but rather an effective theory corresponding to the specific region of the phase diagram we are interested in (which in our case will be the region of high density or chemical potential). Probably the most central quantity in statistical physics is the partition function, which in full glory in QCD is given by:

$$Z = \mathrm{Tr}[e^{-\beta(\hat{H}-\mu\hat{N})}] = N\int D\bar{\Psi}D\Psi DA^a_\mu D\eta D\eta^+ \exp\int_X \mathcal{L} \tag{7}$$

where $\mathcal{L}$ denotes the QCD Lagrangian and η and η^+ denote ghost fields as discussed before. For our effective theory we will need the corresponding expression for non interacting scalar fields, which is given by:

$$Z = \mathrm{Tr}[e^{-\beta(\hat{H}-\mu\hat{N})}] = N\int D\Phi \exp\int_X \mathcal{L} \tag{8}$$

In both expressions, we abbreviated: $\int_X = \int_0^\beta d\tau \int d^3x$, $\beta = \frac{1}{T}$. The integration involving the square of the conjugated momentum π of the Hamiltonian is Gaussian and gives an infinite contribution, which is included in N. At this point, since we later want to take into account meson condensation, we divide our scalar field into a condensate and background fluctuations:

$$\Phi \to \langle\Phi\rangle + \Phi \tag{9}$$

Inserting this ansatz into the Lagrangian we want to consider, yields:

$$\mathcal{L} = -U(\Phi^2) + \mathcal{L}^{(2)} + \mathcal{L}^{(3)} + \mathcal{L}^{(4)} + (...) \tag{10}$$

.

$U(\Phi^2)$then denotes the tree level potential and $\mathcal{L}^{(i)}$ higher order terms in the fluctuations (in case of a ϕ^4 theory we would for example find fluctuations up to the fourth order). Neglecting these fluctuations and considering a condensate, which does not depend on space time, the evaluation of the integral in the exponent of Z becomes trivial: $\int_X \to \frac{V}{T}$. (Keeping terms in the fluctuations would yield additional contributions describing thermal agitations of the mesons). Using the partition function of a system, we can derive any thermodynamic quantity. Since we will follow a Ginzburg Landau approach, we will be specially interested in the grand canonical potential:

$$\Omega = -\frac{1}{\beta}\ln Z \tag{11}$$

The energy density in our case is then simply given by:

$$\frac{\Omega}{V} = -\mathcal{L}(\Phi = \langle\Phi\rangle) = U(\Phi^2) \tag{12}$$

We will later explicitly evaluate this expression for the Lagrangian in a high density effective theory.

1.3 Symmetries in QCD

1.3.1 Gauge symmetry

The invariance of the QCD Lagrangian under $SU(3)_c$ transformations can be checked by applying:

$$\Psi \to U\Psi, \qquad A_\mu \to UA_\mu U^{-1} + \frac{i}{g}U\partial_\mu U^{-1}, \qquad G_{\mu\nu} \to UG_{\mu\nu}U^{-1}, \qquad D_\mu\Psi \to UD_\mu\Psi \tag{13}$$

Since gauge transformations are local, $U \in SU(3)$ depends on space-time: $U = U(\vec{x}, t)$. We will later come back to gauge symmetries (or more precisely their breaking) when discussing the ground state of superconductors.

1.3.2 Flavor symmetries

In the limit of high energies, quark masses are negligible and the QCD Lagrangian is invariant under the chiral symmetry group, which can be characterized as follows: Quark fields $\Psi = [u, d, s, ...]^T$can be decomposed into left handed and right handed fields by using the corresponding projection operators:

$$\Psi = \Psi_L + \Psi_R = P_L\Psi + P_R\Psi \tag{14}$$

$$P_R = \frac{1}{2}(1 + \gamma_5), \qquad P_L = \frac{1}{2}(1 - \gamma_5), \qquad \gamma_5 = i\gamma_0\gamma_1\gamma_2\gamma_3 \tag{15}$$

which indeed satisfy the properties of projection operators:

$$P_{R,L}^2 = P_{R,L}, \qquad P_{R,L}^+ = P_{R,L}, \qquad P_R P_L = 0, \qquad P_R + P_L = 1 \tag{16}$$

Using $\{\gamma_5, \gamma_\mu\} = 0$ we can now decompose the fermionic part of the QCD Lagrangian into:

$$\mathcal{L}_{QCD} = \bar{\Psi}_R(i\gamma^\mu D_\mu + \gamma^0\mu)\Psi_R + \bar{\Psi}_L(i\gamma^\mu D_\mu + \gamma^0\mu)\Psi_L - \bar{\Psi}_R M\Psi_L - \bar{\Psi}_L M\Psi_R \tag{17}$$

M denotes the mass matrix and is given by $M = diag(m_u, m_d, m_s)$ in case of three flavors.

Since mass terms obviously mix left and right handed flavors, chiral symmetry is explicitly broken by non vanishing quark masses. One can formulate this statement in a more physical way: If chiral symmetry were always conserved, we would expect, that any (strong interacting) particle comes with a chiral partner of equal mass and opposite parity. However, these partner particles are not observed in nature. Hence the QCD vacuum is of lower symmetry. We will now analyze this in more detail.

The full symmetry-group 3 flavor massless QCD is given by:

$$U(3)_L \otimes U(3)_R = SU(3)_L \otimes SU(3)_R \otimes U(1)_L \otimes U(1)_R \tag{18}$$

In order to save the invariance of the mass term in the Lagrangian, we would need to set

$$U(3)_L = U(3)_R := U(3)_{R+L} = U(3)_V, \qquad m_u = m_d = m_s \tag{19}$$

The first condition corresponds to a simultaneous rotation of left and right handed flavors in the same direction and is referred to as vector-rotation. We now have:

$$\bar{\Psi}\Psi = \bar{\Psi}_R U_V^+ U_V \Psi_L + \bar{\Psi}_L U_V^+ U_V \Psi_R = \bar{\Psi}_R\Psi_L + \bar{\Psi}_L\Psi_R = \bar{\Psi}\Psi \tag{20}$$

In case of different masses for all flavors, $m_u \neq m_d \neq m_s$, even the vector symmetry becomes only an approximate one. The only symmetry remaining is a separate $U(1)_V$ symmetry for each quark flavor. The symmetry of vector transformations $SU(3)_V$ is often referred to as isospin and is, although being only approximate, often used to describe the ordering mesons and baryons in corresponding isospin multiplets [1]. In order to cover the entire group of $U(3)_L \otimes U(3)_R$, we also need to take into account the axial-vector symmetry, in which left handed and right handed flavors rotate in opposite directions. In total, we perform a change of basis in flavor space, given by the following set of transformations:

$$V \to L + R, \qquad A \to L - R \tag{21}$$

$$SU(3)_L \otimes SU(3)_R \otimes U(1)_L \otimes U(1)_R \equiv SU(3)_V \otimes SU(3)_A \otimes U(1)_V \otimes U(1)_A \tag{22}$$

We list all symmetry transformations and the corresponding Noether currents in table 2.

[1] More precisely, isospin is a SU(2) subgroup of SU(3). In principle we can pick out any two entries from the flavor vector $\begin{pmatrix} u \\ d \\ s \end{pmatrix}$ in order to construct an SU(2) sub algebra. In addition to isospin (u,d) there are also the sub algebras of U (u,s) and V (d,s) -spin. It is clear that, taking into account the quark masses given in table (1), the isospin is the "best conserved" symmetry ($\frac{\Delta m}{m} \backsim 1\%$). The generators of isospin simply are $T_1 = \frac{\lambda_1}{2}$, $T_2 = \frac{\lambda_2}{2}$ and $T_3 = \frac{\lambda_3}{2}$ or equivalently using ladder operators: T_3 and $T_\pm = (T_1 \pm iT_2)$. Adding the hypercharge $Y = \frac{2}{\sqrt{3}}T_8$ (consider that both, λ_3 andλ_8 are diagonal matrices and hence commute), we can construct all multiplets within $Y - T_3$ diagrams, which is the conventional way to illustrate the ordering of hadrons. Using ladder operators then allows to reach all possible states within a multiplet. Each multiplet represents states of fixed isospin and parity. The flavor structure of quark-anti-quark states (Mesons) can be decomposed as: $[\bar{3}] \otimes [3] = [8] \oplus [1]$ and states consisting of three quarks (Baryons) as: $([\bar{3}] \otimes [3]) \otimes [3] = ([10] \oplus [8]) \oplus ([8] \oplus [1])$. For a more than complete analysis refer to [1].

transformation	Noether current	symmetry
$\Psi \rightarrow \Psi^{'} = e^{i\alpha}\Psi$	$J^{\mu}_{V,0} = \bar{\Psi}\gamma^{\mu}\Psi$	$U_V(1)$ vector
$\Psi \rightarrow \Psi^{'} = e^{i\alpha_a\lambda_a}\Psi$	$J^{\mu}_{V,a} = \bar{\Psi}\gamma^{\mu}\lambda_a\Psi$	$SU_V(3)$ axial-vector
$\Psi \rightarrow \Psi^{'} = e^{i\alpha\gamma_5}\Psi$	$J^{\mu}_{A,0} = \bar{\Psi}\gamma^{\mu}\gamma_5\Psi$	$U_A(1)$ vector
$\Psi \rightarrow \Psi^{'} = e^{i\alpha_a\lambda_a\gamma_5}\Psi$	$J^{\mu}_{A,a} = \bar{\Psi}\gamma^{\mu}\gamma_5\lambda_a\Psi$	$SU_A(3)$ axial-vector

Table 2: List of symmetry transformations in 3 flavor QCD.

$J^{\mu}_{V,a}$ corresponds to the conservation of isospin, $J^{\mu}_{V,0}$ to the conservation of baryon number. The latter is always an exact symmetry. Lets now investigate the axial-vector symmetry in more detail:

Mass terms explicitly break the axial-vector symmetry, even in the case of $m_u = m_d = m_s$, which is what we expect since this explicit breaking through mass terms also occurs for an independent left and right handed symmetry which is equivalent as indicated in equation (22). Since vector rotations are conserved in case of $m_u = m_d = m_s$, the axial-vector part now has to cover this explicit breaking. To check this we set:

$$U_R = U_V U_A, \qquad U_L = U_V U_A^{+} \tag{23}$$

where we have explicitly used the fact, that vector symmetries affect left handed and right handed fields in the same way, whereas axial symmetries affect them in the opposite way. With these properties, we find:

$$U_A = U_V^{+} U_R = U_L^{+} U_V \tag{24}$$

$$\bar{\Psi}_L\Psi_R \rightarrow \bar{\Psi}_L U_L U_R \Psi_R = \bar{\Psi}_L U_A U_V^{+} U_V U_A \Psi_R = \bar{\Psi}_L U_A U_A \Psi_R \tag{25}$$

$$\bar{\Psi}_R\Psi_L \rightarrow \bar{\Psi}_R U_R^{+} U_L \Psi_L = \bar{\Psi}_R U_A^{+} U_V^{+} U_V U_A^{+} \Psi_L = \bar{\Psi}_R U_A^{+} U_A^{+} \Psi_L \tag{26}$$

which confirms our assumption. Finally, even the axial $U(1)_A$ symmetry is broken down to the discrete subgroup of $\mathbb{Z}_A(6)$ through a quantum effect, although the corresponding symmetry transformation leaves the Lagrangian invariant. Such a symmetry breaking is hence referred to as "anomalous" and was first explained by t'Hooft by the use of instantons [2][3]. This effect becomes visible in the non conservation of the singlet axial-current:

$$\partial_{\mu} J^{\mu}_{0,A} = -\frac{g^2 N_f}{16\pi^2} G^a_{\mu\nu} \widetilde{G}^{\mu\nu}_a \tag{27}$$

where $\widetilde{G}^{\mu\nu} = \frac{1}{2}\epsilon^{\mu\nu\rho\sigma} G_{\rho\sigma}$ denotes the dual field strength tensor. We summarize all results of this section in the following diagram:

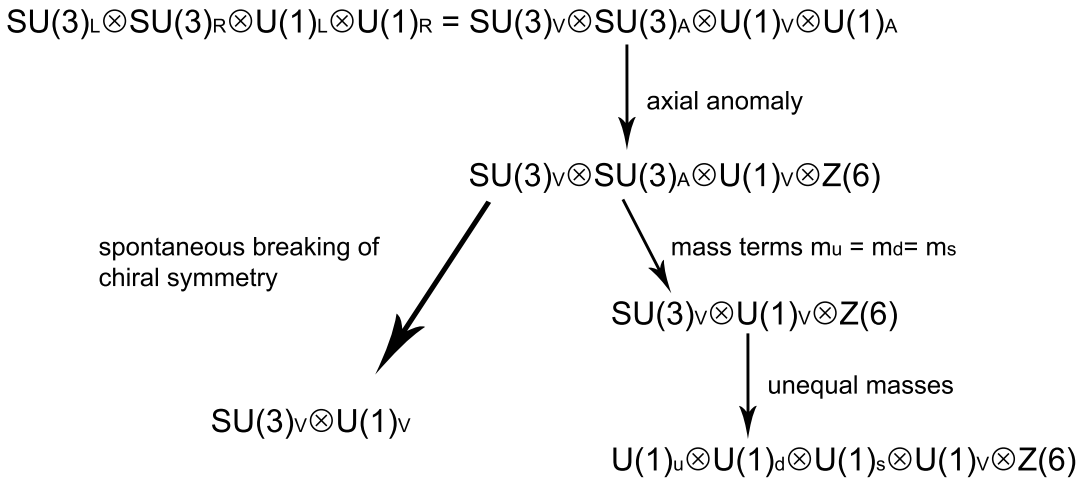

Figure 1: Schematic of symmetry breaking patterns. Spontaneous symmetry breaking differs essentially from the explicit symmetry breaking discussed in this section and will be discussed later.

1.4 Non perturbative aspects of QCD

1.4.1 Asymptotic freedom and Confinement:

Probably the most striking feature of QCD is the fact, that the strength of the interaction between quarks which is mediated by gluons approaches zero in the limit of high momentum transfer or small distances [4][5]. Another way of characterizing this phenomenon is by introducing the concept of a running coupling constant $\alpha_{QCD} = \alpha(q^2)$ depending on the momentum transfer q. The first order approximation of α_{QCD} is then given by:

$$\alpha(t) = \frac{\alpha}{1 - (\frac{\alpha}{\pi})b_1 t} \tag{28}$$

where $t = \frac{1}{2} ln(\frac{q^2}{\Lambda^2_{QCD}})$ and $\alpha = \alpha(t = 0)$.

Λ_{QCD} denotes the QCD scale which is experimentally determined to be about 200MeV. The coefficient b_1 can be calculated perturbatively where one finds $b_1 < 0$, which reflects asymptotic freedom ($\alpha(t)$ decreases with increasing t), whereas $b_1 > 0$ for example in the case of QED. (Extensive treatment of asymptotic freedom in terms of renormalization-group theory can be found for example in [6][7]). Therefore we find the usual screening-effect of electromagnetic forces in QED but anti-screening of color charges in QCD.

At low energies, quarks are hence strongly correlated and an additional experimental constraint is given by the fact, that we observe only color-neutral hadrons (strong interacting particles), namely mesons and baryons, in accelerator experiments. While mesons remain color neutral by pairing quarks and anti-quarks such that colors are always combined with the respective anti-color, baryons consist of three quarks and mix colors such that the resulting color is white (completely analogous to regular colors, where for example the addition of red, green and blue yields white). The mechanism, that confines quarks into Mesons and Baryons is still poorly understood and cannot be explained by perturbative means.

1.4.2 Spontaneous breaking of chiral symmetry

The extraordinary small mass of pions which is about 140MeV led to speculations whether mesons might actually be Goldstone Bosons of chiral symmetry breaking. The Goldstone realization of symmetry breaking differs essentially from the ones discussed in chapter 2. We shall categorize symmetry breaking in the frame of this works as follows:

- explicit symmetry breaking: The symmetry is broken on the level of the Lagrangian. This scenario was discussed in connection with the breaking of chiral symmetry through mass terms.
- anomalous symmetry breaking: The Lagrangian is invariant under a symmetry transformation, but the symmetry is still broken due to quantum effects. This scenario was discussed in connection with the symmetry of $U(1)_A$.
- spontaneous symmetry breaking: The Lagrangian is invariant under a symmetry transformation, but the ground state is not. In this case, the Goldstone-theorem tells us to expect Dim(H)-Dim(G) massless Goldstone-particles where H and G are the symmetry groups of the Lagrangian and the ground state.

The spontaneous breaking of chiral symmetry is somewhat more complicated. Since, as discussed before, chiral symmetry is only approximate, its breaking is a dynamical matter. The explicit breaking through quark masses, even though very small, leads to small masses for the Goldstone bosons. Goldstone modes with non vanishing masses are generally referred to as pseudo-Goldstone modes.

We now have to determine the symmetry groups G and H. Spontaneous breaking of chiral symmetry is induced by a condensate of the form $\langle \bar{\Psi}_L \Psi_R \rangle$ and the corresponding symmetry-breaking pattern is given by:

$$SU(3)_L \otimes SU(3)_R \otimes U(1)_L \otimes U(1)_R \rightarrow SU(3)_{L+R} \otimes U(1)_{L+R} \tag{29}$$

Consequently we find: Dim(H)=8+8 , Dim(G)=8 and Dim(H)-Dim(G)=8 in case of the breaking of SU(3), as well as Dim(H)-Dim(G)=1 in case of U(1). The resulting 8+1 pseudo Goldstone-modes are given by the meson nonet, where the η' mode corresponds to the breaking of the chiral U(1) symmetry and is unusually heavy due to the axial anomaly (see chapter 2). We can relate the non conservation of the axial current discussed in chapter 2 to the small pion masses by considering $\langle 0 \left| J^k_{5\mu}(x) \right| \pi^J \rangle = i\delta_{j,k} f_\pi p_\mu e^{-ipx}$, where j and k denote isospin indices and $f_\pi \approx 93$ MeV is the pion decay constant (to simplify matters we have restricted ourselves to chiral SU(2) here). From this ansatz, we can see that conservation of the axial current is only possible in the case of vanishing pion masses:

$$\langle 0 \left| \partial^\mu J^k_{5\mu}(x) \right| \pi^J \rangle = \delta_{j,k} f_\pi p^\mu p_\mu e^{-ipx} = \delta_{j,k} m_\pi^2 e^{-ipx} \tag{30}$$

The Meson nonet is conventionally illustrated within an Isospin-Hypercharge diagram:

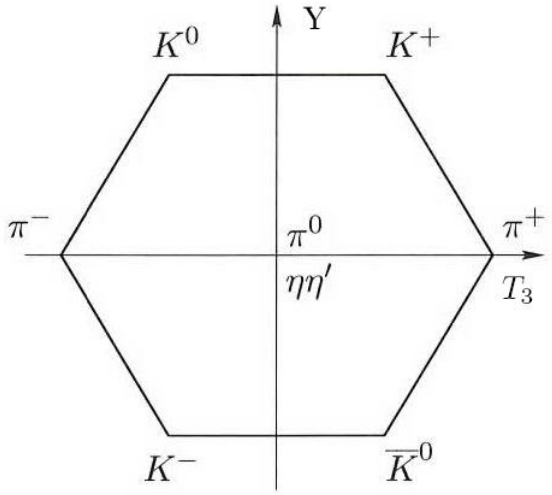

Figure 2: The meson nonet in the Y-T3 plane. Mesons decompose into isospin multiplets according to $[3] \otimes [\bar{3}] \rightarrow [8] \oplus [1]$.

The SU(3) matrix, containing all these mesonic fields θ_a, a ranging from 1 to 9, is given by:

$$U = e^{i\theta_a \lambda_a / f_\pi} \tag{31}$$

with the meson fields θ_a and Gell-Mann matrices λ_a. Rows of the exponent of this matrix carry left handed flavor, while columns carry right handed anti-flavor. We can now easily read of the particle content (for example $\pi^+ \sim \bar{d}u$):

$$\theta_a \lambda_a = \begin{pmatrix} \frac{\pi^0}{\sqrt{2}} + \frac{\eta}{\sqrt{6}} & \pi^+ & K^+ \\ \pi^- & -\frac{\pi^0}{\sqrt{2}} + \frac{\eta}{\sqrt{6}} & K^0 \\ K^- & \bar{K}^0 & -\sqrt{\frac{2}{3}}\eta \end{pmatrix} \tag{32}$$

An instructive effective model to study the spontaneous breaking of chiral symmetry in the simplified case of $SU(2)_L \otimes SU(2)_R$ is the so called linear-σmodel. In this model, the elementary fields are provided by the nucleon-doublets Ψ , a triplet pion field π^i and a scalar field σ, all of which are massless and hence represent "real" Goldstone-modes .

The corresponding Lagrangian is given by :

$$\mathcal{L} = \bar{\Psi}(i\gamma^\mu \partial_\mu - g\sigma + i\vec{\tau}\vec{\pi}\gamma_5)\Psi + \frac{1}{2}(\partial_\mu \sigma \partial^\mu \sigma + \frac{1}{2}\partial_\mu \vec{\pi}\partial^\mu \vec{\pi} + \frac{\mu^2}{2}(\sigma^2 + \pi^2) - \frac{\lambda}{4}(\sigma^2 + \pi^2)^2 \tag{33}$$

where the effective potential V is represented by the last two terms and we can observe spontaneous symmetry breaking for $\mu^2 > 0$ (see figure 3). For more details see for example reference [7].

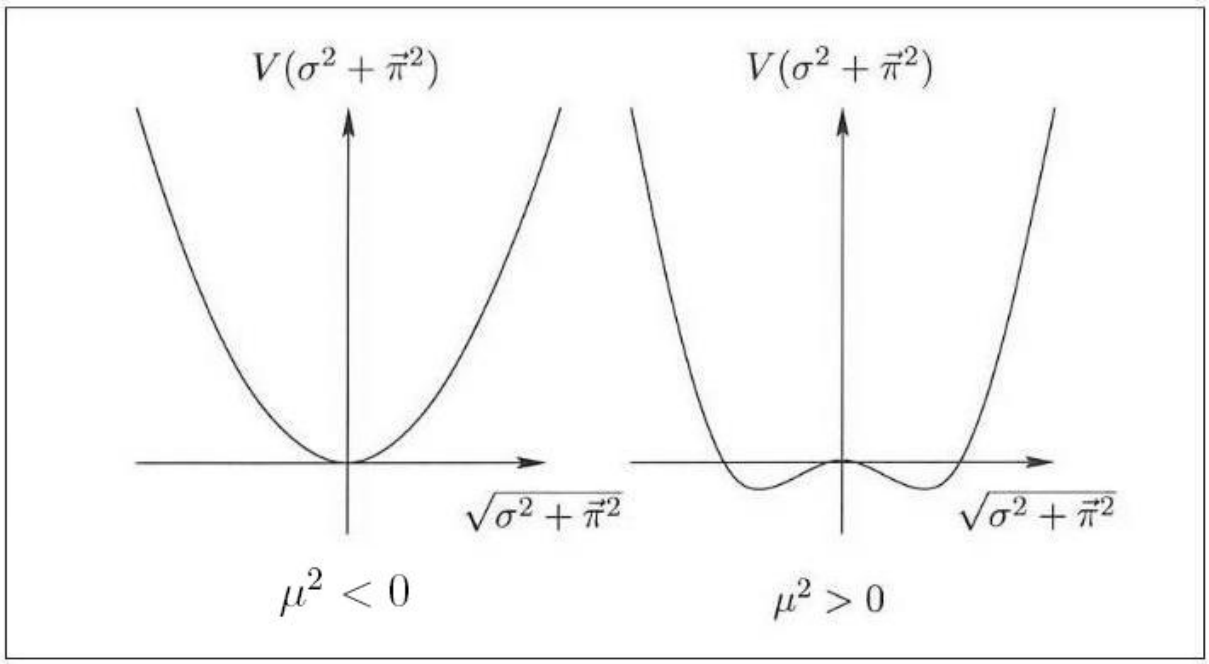

Figure 3: Illustration of the spontaneous breaking of chiral symmetry in the linear sigma model. The minimum of the potential energy is fixed by $\sigma^2 + \vec{\pi}^2 = \frac{\mu^2}{\lambda}$ which describes of sphere of degenerate massless ground states. If we introduce a linear shift to the σ fields $\sigma \to \bar{\sigma} = \sigma - v$ and plug this new field into the effective Lagrangian, we now find a mass term $2\mu^2\bar{\sigma}^2$, whereas the pion field remains exactly massless.(which is still not entirely true since pions are unusual light but not massless particles). One illustrative way to understand this effect is to imagine, that the mexican-hat potential is now tilted on one side.

At the end of this chapter, we descirbe a chiral effective Lagrangian which is invariant under the symmetry group G. As discussed before, we often rely on effective Lagrangians according to the specific energy scale we want to consider. Low energy effective theories have been used with great success for example in nuclear physics. At this energy scale we have to consider Mesons and Baryons rather than Quarks and Gluons. At first sight, building a Lagrangian invariant under G seems not to be an appropriate choice in a low energy regime, since nonzero quark masses break chiral symmetry. Nevertheless, quark masses are small compared to the specific scale of chiral symmetry breaking $4\pi f_\pi \backsim 1GeV$ and we can still consider chiral symmetry as approximate. An effective Lagrangian is then given by [8]:

$$\mathcal{L} = \frac{f_\pi^2}{4}\mathrm{Tr}[\partial_\mu U \partial^\mu U^+] + c\mathrm{Tr}[M^+U + MU^+] + (.....) \tag{34}$$

where we have neglected higher order mass terms. The trace is taken over flavor space. In such a low density effective theory, one should also consider the existence of Baryons (which interact through the exchange of mesons). Hence the full effective Lagrangian would be given by $\mathcal{L} = \mathcal{L}_{Meson} + \mathcal{L}_{Baryon} + \mathcal{L}_{int}$. A list of all terms included in $\mathcal{L}_{int}$ would be rather lengthy and complicated, see for example [9]. However, in our discussion of the phase diagram we will not include Baryons. We shall later also consider an high density effective theory and compare it to the low density counterpart.

1.5 High density quark matter

1.5.1 Superconductivity in high density quark-matter

We now turn to the region of large chemical potential μ. As mentioned already in the introduction, we expect to find asymptotically free quarks, which are in a state of superconductivity. Due to asymptotic freedom, superconductivity in high density quark matter can be understood theoretically from (perturbative) first principle calculations. Before asking for the explicit ground state in this regime, we quickly review the definition superconductivity, which is best given by Cooper's theorem. To that end, we consider a system of fermions with a chemical potential μ and zero temperature,where the free energy is given by:

$$\Omega = E - \mu N \tag{35}$$

We can quickly check, that adding another fermion at the Fermi surface (which means with $E_{fermion} = \mu$) does not change the overall energy of the system: $\Omega^{'} = (E + \mu) - \mu(N + 1) = \Omega$. If we now add an (however small) attractive interaction to the fermions, adding two fermions will automatically reduce the free energy of the system, because the attractive interaction will lead to an energy gain from the binding energy. The original Fermi surface will become unstable and a new ground state is formed which contains pairs of fermions rather than single independent ones,and these fermion pairs can formally be viewed as bosons (Note however, that the fermion-fermion correlations exists in momentum space, not in real space). We are hence dealing with a Bose condensate.

This mechanism is general and holds true for any fermionic system. The only difference arises in the way the attractive interaction is provided: In a solid state body, we need a complex mechanism of electron-phonon interactions in order to observe superconductivity among electrons (direct Coulomb interaction between electrons is repulsive), whereas in quark-matter the attractive force is simply given by single gluon exchange. Applying this principle for example on neutrons, protons and quarks we expect to find superfluidity (neutrons) as well as superconductivity. In the case of quarks we will have to be very careful in defining superconductivity since we will not only have to deal with electric charges but also with color charges.

The finite amount of energy, required to break Cooper pairs is given by an energy "gap" $\triangle$ which appears in the single particle dispersion-relation:

$$\epsilon = \sqrt{(E_k - \mu)^2 + \triangle^2}, \qquad E_k = \sqrt{k^2 + m^2} \tag{36}$$

Setting $\triangle = 0$ we find $\epsilon = \pm(E_k - \mu)$ which is the expected dispersion relation for particle/hole systems. As we can see for large μ, quark matter will only contain quarks and no anti-quarks since the amount of energy required to excite anti-quarks increases with μ, and we are hence looking for an attractive channel between quarks.

As stated before, the energy gap $\triangle$ in equation (36) can be computed from first principles in (asymptotically) high density quark matter and is given by [9],[10]:

$$\triangle = 2b\mu exp(-\frac{3\pi^2}{\sqrt{2}g}), \qquad b = 256\pi^4(\frac{2}{N_f g^2})^{5/2} \tag{37}$$

However, a weak coupling calculation of $\triangle$ can strictly only be considered valid at chemical potentials of the order of $\mu \gtrsim 10^8 MeV$ (whereas the most dense natural systems after black holes are compact stars, which come with a quark chemical potential of the order of at most $\mu \lesssim 500 MeV$). Since going from a superconducting to a non-superconducting phase involves a phase transition, it must be related to the breakdown of a symmetry. We will hence now investigate symmetries and breaking patterns of high density quark matter.

1.5.2 Basic properties of color-flavor-locked (CFL) quark matter

The Cooper pair order parameter, given by a quark-quark two point function $\langle\Psi\Psi\rangle$,obviously breaks color symmetry $SU(3)_C$ spontaneously analogously to the way the transition to superconductivity of electrons, which breaks $U(1)_{em}$,which justifies the terminology of color superconductivity. We will now investigate the color flavor structure of this condensate. As mentioned before, in the case of asymptotically free quarks, the attractive interaction is provided by single gluon exchange. In terms of the color gauge group $SU(3)_C$, quark-quark pairing is given by:

$$[3]_C \otimes [3]_C = [\bar{3}]^A_C \oplus [6]^S_C \tag{38}$$

At the left side, the quarks are given in their fundamental representation. The right side shows possible channels for interactions: An antisymmetric anti-triplet channel, which is attractive, and a symmetric sextet channel, which is repulsive and hence not of any interest. In the high density regime we can also consider chiral symmetry to be restored and therefore find the same result for $SU(3)_f$ as for $SU(3)_C$:

$$[3]_{L,R} \otimes [3]_{L,R} = [\bar{3}]^A_{L,R} \oplus [6]^S_{L,R} \tag{39}$$

Taking into account, that cooper pairing is preferred in the antisymmetric spin-0 channel and that the overall wave function of the cooper pairs (spin+flavor+color) must be antisymmetric, we can conclude that also the flavor structure of the condensate must be antisymmetric, which leads us to the following color-flavor structure of the order parameter:

$$\langle\Psi\Psi\rangle \in [\bar{3}]^A_c \otimes [\bar{3}]^A_f \tag{40}$$

More explicitly, we can now choose an antisymmetric basis for both indices and write:

$$\left\langle \Psi^\alpha_i C\gamma_5 \Psi^\beta_j \right\rangle \propto \epsilon^{\alpha\beta a}\epsilon_{ijb}\Phi^b_a \tag{41}$$

On the left we have used the charge conjugation matrix $C = i\gamma^2\gamma^0$ in order to take care of the Dirac (spin) degree of freedom. The 3×3 matrix Φ^b_a on the right side now determines the specific color-flavor structure within the given antisymmetric basis. From this ansatz, it becomes clear that we could in principle construct many different color superconducting phases by choosing different structures for the matrices Φ^b_a. In some phases, all tnine color/flavor combinations contribute to the condensation, in others (such as 2SC), one flavor remains unpaired. We will now focus on color-flavor-locking (CFL) which can be shown to be the favored ground state at high densities [11],[12],[13],[14]. The specific ansatz for Φ^b_a CFL is given by:

$$\Phi^b_a = \delta^b_a, \qquad \left\langle \Psi^\alpha_i C\gamma_5 \Psi^\beta_j \right\rangle \propto \epsilon^{\alpha\beta a}\epsilon_{ija} \tag{42}$$

The resulting 9×9 matrix is explicitly given by:

$$\left\langle \Psi^\alpha_i C\gamma_5 \Psi^\beta_j \right\rangle \propto \begin{pmatrix} 0 & 0 & 0 & 0 & -1 & 0 & 0 & 0 & -1 \\ 0 & 0 & 0 & 1 & 0 & 0 & 0 & 0 & 0 \\ 0 & 0 & 0 & 0 & 0 & 0 & 1 & 0 & 0 \\ 0 & 1 & 0 & 0 & 0 & 0 & 0 & 0 & 0 \\ -1 & 0 & 0 & 0 & 0 & 0 & 0 & 0 & -1 \\ 0 & 0 & 0 & 0 & 0 & 0 & 0 & 1 & 0 \\ 0 & 0 & 1 & 0 & 0 & 0 & 0 & 0 & 0 \\ 0 & 0 & 0 & 0 & 0 & 1 & 0 & 0 & 0 \\ -1 & 0 & 0 & 0 & -1 & 0 & 0 & 0 & 0 \end{pmatrix} \tag{43}$$

We also can write this result by defining our antisymmetric basis as:

$$(J^a)^{\alpha\beta} = -i\epsilon^{\alpha\beta a}, \qquad (I_b)_{ij} = -i\epsilon_{ijb} \tag{44}$$

We then find the following compact relation:

$$\left\langle \Psi_i^\alpha C\gamma_5 \Psi_j^\beta \right\rangle \propto \vec{J}\cdot\vec{I} = i \begin{pmatrix} 0 & -I_3 & I_2 \\ I_3 & 0 & -I_1 \\ -I_2 & I_1 & 0 \end{pmatrix} \tag{45}$$

We label rows and columns with nine quarks in the following fashion: ru, rd,rs,gu,gd,gs,bu,bd,bs (where ru denotes a red up quark etc) and can immediately read up all non vanishing pairings. As we can see, only the following combinations are possible: ru-gu, bu-rs, bd-gs, ru-gd-bs

The corresponding quasi-particle dispersion relation is given by:

$$\epsilon_{k,r} = \sqrt{(k-\mu)^2 + \lambda_r \triangle^2} \tag{46}$$

By λ_r we denote the eigenvalues of the operator $L = (\vec{J}\cdot\vec{I})^2$ and by $\triangle$ the expression for the superconducting gap (37).

1.5.3 Chiral symmetry breaking in CFL

Having determined the specific color-flavor structure of the CFL order parameter, we need to investigate the pattern of the induced symmetry breaking. In this respect it is necessary to apply symmetry transformations on the generators J and I as follows:

$$J^A I_A \rightarrow (UJ^A U)(VI_A V^T) \tag{47}$$

U and V are the corresponding SU(3) color and flavor transformations, explicitly: $U = e^{i\Phi_a^C T_a}$, $V = e^{i\Phi_a^f T_a}$. We now have:

$$(U_{\alpha\beta}\epsilon_{\beta\gamma A}U^T_{\gamma\delta})(V_{ij}\epsilon_{ijA}V^T_{kl}) = U_{\alpha\beta}U^T_{\gamma\delta}V_{ij}V^T_{kl}(\delta_{\beta j}\delta_{\gamma k} - \delta_{\beta k}\delta_{\gamma j}) = U_{\alpha j}U^T_{k\delta}V_{ij}V^T_{kl} - U_{\alpha k}U^T_{j\delta}V_{ij}V^T_{kl} \tag{48}$$

Demanding invariance, we have to choose U and V such that the right hand side of the above equation is equal to $\delta_{\beta j}\delta_{\gamma k} - \delta_{\beta k}\delta_{\gamma j}$. Rearranging U and V we find:

$$U_{\alpha j}U^T_{k\delta}V_{ij}V^T_{kl} - U_{\alpha k}U^T_{j\delta}V_{ij}V^T_{kl} = U_{\alpha j}V^T_{ji}U_{\delta k}V^T_{kl} - U_{\alpha k}V^T_{kl}U_{\delta j}V^T_{ji} \tag{49}$$

which yields the desired result in case of $V = U^*$. We are also later going to make use of the explicit structure of $\phi_a T_a$, given by:

$$\phi_a T_a = \frac{1}{2}\begin{pmatrix} \phi_3 + \frac{1}{\sqrt{3}}\phi_8 & \phi_1 - i\phi_2 & \phi_4 - i\phi_5 \\ \phi_1 + i\phi_2 & -\phi_3 + \frac{1}{\sqrt{3}}\phi_8 & \phi_6 - i\phi_7 \\ \phi_4 + i\phi_5 & \phi_6 + i\phi_7 & -\frac{2}{\sqrt{3}}\phi_8 \end{pmatrix} \tag{50}$$

Hence, for any real matrix element $(\phi_a T_a)^{Re}_{i,j}$ we have $V \equiv U$ whereas for imaginary elements $(\phi_a T_a)^{Im}_{i,j}$ we need $V = U^*$. The CFL diquark condensate breaks chiral, color and baryon conservation symmetries according to:

$$SU(3)_C \otimes SU(3)_L \otimes SU(3)_R \otimes U(1)_B \rightarrow SU(3)_{L+R+C} \otimes Z(2) \tag{51}$$

where $Z(2)$ denotes a discrete subgroup of $U(1)$. In this pattern we have already neglected the group of$U_A(1)$, which is broken anyway due to the axial anomaly. Regarding chiral symmetry, this breaking pattern is exactly the same as in a low density nuclear matter regime where chiral symmetry breaking is induced by a condensate of the form $\left\langle \bar{\Psi}_R \Psi_L \right\rangle$ rather then $\langle \Psi_L \Psi_L \rangle$ or $\langle \Psi_R \Psi_R \rangle$. The fundamental difference

is given by the color degree of freedom: In order to leave the order parameter invariant, a color-rotation has to be compensated by equal right and left handed rotations.

This motivates the declaration of "color-flavor-locking". We will now briefly summarize the most important consequences of the above breaking pattern:

- Due to spontaneous chiral symmetry breaking, we expect to find an octet of Goldstone modes in analogy to the breaking induced by $\langle \bar{\Psi}_R \Psi_L \rangle$. Especially at lower densities, where we the effect of strange quarks increases, we expect kaon condensation.

- The gauge group $SU(3)_c$ is completely broken. Since spontaneous breakdown of a gauge symmetry leads to masses for the gauge bosons, we expect to find Meissner masses for all 8 gluons (just like the photon acquires a Meissner mass due to the breaking of $U(1)_{em}$).

- The breakdown of baryon conservation number $U(1)_B$,which is always an exact symmetry of QCD(even at lower densities), gives rise to one massless Goldstone mode and CFL becomes a super-fluid.

1.5.4 Kaon condensation in CFL

In the same way the chiral field U was embedded in an effective theory in equation (34), we can now set up an high density effective theory around a new chiral field Σ. In this case, Σ is explicitly given by

$$\Sigma = \frac{d_L^+ d_R}{d^2}, \quad \epsilon U(3) \tag{52}$$

By $d_{L,R}$ we denote the diquark two-point functions $\langle \Psi_{R,L} \Psi_{R,L} \rangle$ with the symmetry properties discussed in the last section. Σ contains nine degrees of freedom, one of which is usually ignored since it corresponds to η' particle, which is relatively heavy due to the anomalous breaking of $U(1)_A$. We can identify the 8 remaining mesons with the meson octet also obtained for nuclear matter in figure(2). Both meson fields are very similar, in particular they posses the same quantum numbers. However, we have to consider one essential difference: While a "regular" meson is composed of a quark-anti-quark pair, CFL mesons are composed of two diquarks (which means two fermions and two fermion-holes). The neutral kaon K^0 for example is composed of $K^0 \propto \bar{s}d$ while the CFL counterpart is given by $\tilde{K}^0 \propto \bar{u}\bar{s}du$. From this we can deduce the following equivalences:

$$\begin{pmatrix} u \\ d \\ s \end{pmatrix} \rightarrow \begin{pmatrix} \bar{d}\bar{s} \\ \bar{u}\bar{s} \\ \bar{u}\bar{d} \end{pmatrix} \tag{53}$$

which reflects the antisymmetric anti-triplet representation of diquark condensates, discussed before. A meson in this sense will differ significantly in mass and also decay constants will have to be recalculated: The "normal" mass ordering given by $m_u < m_d < m_s$ is now replaced by $m_d m_s > m_u m_s > m_u m_d$ which means, that also the mass ordering of the Goldstone modes has to be rearranged. In particular, the neutral kaon is now lighter than the neutral pion since we now find:

"normal mesons": $m_{\pi^o} \propto (m_u + m_d) \quad m_{K^0} \propto (m_s + m_d) \quad \rightarrow m_{\pi^0} < m_{K^0}$

"CFL mesons": $m^2_{\pi^0} \propto (m_d m_s + m_u m_s) \quad m^2_{K^0} \propto (m_u m_d + m_u m_s) \quad \rightarrow m_{\pi^0} > m_{K^0}$

A more detailed analysis of the inverse mass ordering is given in [14]. A complete evaluation of the mass-term is lengthy and given in appendix [1]. In our analysis of meson condensation in CFL we will restrict ourselves to neutral kaons for the following reasons:

1. Charged mesons would require the presence of electrons or positrons to establish electric neutrality, which disfavors charged condensates.
2. If we go down from asymptotically high densities to lower densities, we expect the effects of the strange quark mass to be come important. The system is then expected to react by developing a meson condensates. The neutral kaon is the lightest particle to produce an effective chemical potential proportional to m_s^2. (see for example reference [14] , [15] ,[16]).
3. The η' particle is ignored in this analysis, since it is very heavy due to the explicit breaking of $U(1)_A$.

Formally, restricting ourselves to neutral kaons means setting all fields except for the kaon fields in (32) equal to zero (the structure is of course the same as in (50)):

$$Q = \phi_a \lambda_a = \begin{pmatrix} 0 & 0 & \phi_4 - i\phi_5 \\ 0 & 0 & \phi_6 - i\phi_7 \\ \phi_4 + i\phi_5 & \phi_6 + i\phi_7 & 0 \end{pmatrix} \tag{54}$$

Using [9]:

$$\cos Q = 1 - \frac{Q^2}{\phi^2}(1 - \cos\phi), \qquad \sin Q = \frac{Q}{\Phi}\sin\phi, \qquad \phi = \sqrt{\phi_4^2 + \phi_5^2 + \phi_6^2 + \phi_7^2} \tag{55}$$

and restricting ourselves to neutral Kaons ($\phi_4 = \phi_5 = 0$), we find:

$$\Sigma = \begin{pmatrix} 1 & 0 & 0 \\ 0 & \cos\phi & i\sin\phi \\ 0 & i\sin\phi & \cos\phi \end{pmatrix} \tag{56}$$

A nonzero ϕ introduces a relative rotation between left- and right-handed diquarks. This rotation does not change the energy of the CFL ground state in the symmetric case of vanishing quark masses. Only with nonzero quark masses the energy is changed and a meson condensate becomes possible. The fields ϕ_6 and ϕ_7 appear in the exponent of the unitary matrix $\Sigma = e^{iQ} = cosQ + isinQ$. We can now use this result to introduce kaon condensation in a high density effective theory.

1.5.5 High density effective theory

A high density equivalent to the chiral effective Lagrangian introduced in (1.4.2) is for example provided in [16],[18]. The effective Lagrangian for the chiral field Σ is given by:

$$\mathcal{L}_{\text{eff}} = \frac{f_\pi^2}{4}\text{Tr}[\nabla_0\Sigma\nabla_0\Sigma^+ - v_\pi^2\partial_i\Sigma\partial_i\Sigma^+] + B[M\Sigma^+ + M^+\Sigma] + \frac{af_\pi^2}{2}\text{det}M\,\text{Tr}[M^{-1}(\Sigma + \Sigma^+)] \tag{57}$$

Weak-coupling calculations give the following values for the constants [16]:

$$f_\pi^2 = \frac{21 - 8\ln 2}{18}\frac{\mu_q^2}{2\pi^2}, \qquad v_\pi^2 = \frac{1}{3}, \qquad a = \frac{3\Delta^2}{\pi^2 f_\pi^2}, \qquad B = c\left(\frac{3\sqrt{2}\pi}{g}\Delta\,\frac{\mu_q^2}{2\pi^2}\right)^2\left(\frac{8\pi^2}{g^2}\right)^6\frac{\Lambda_{\text{QCD}}^9}{\mu_q^{12}} \tag{58}$$

Here, μ_q is the quark chemical potential, Δ the superconducting gap parameter, $c \simeq 0.155$, g the strong coupling constant, and Λ_{QCD} the QCD scale factor. An important contribution to the effective Lagrangian is given by promoting the time derivatives to covariant derivatives:

$$\nabla_0\Sigma \equiv \partial_0\Sigma + i[A, \Sigma], \qquad A \equiv -\frac{MM^+}{2\mu_q} \tag{59}$$

Inserting this expression into the Lagrangian, and evaluating as discussed in chapter (1.2), where we use (56) for the chiral field and $diag(m_u, m_d, m_s)$ for the quark masses, we find:

$$V(\phi) = -\frac{f_\pi^2}{2}\mu^2\sin^2\phi + f_\pi^2 m_{K^0}^2(1 - \cos\phi) \tag{60}$$

Here, μ denotes the kaon chemical potential:

$$\mu^2 = (\frac{m_s^2 - m_d^2}{2p_f})^2 \tag{61}$$

and the effective kaon mass squared is given by:

$$m_{K^0}^2 \equiv \frac{2B(m_d + m_s)}{f_\pi^2} + am_u(m_s + m_d) \tag{62}$$

In equation (60) we have already subtracted the vacuum contribution V(0). The kaon mass squared receives an instanton contribution linear in the quark masses and a contribution quadratic in the quark masses. In the weak-coupling limit at very high densities,$\mu_q \gg \Lambda_{\mathrm{QCD}}$, the instanton contribution is negligible since $U(1)_A$ is effectively restored. In this case the term $M^{-1}\det M$ becomes dominant and the inverse meson mass ordering discussed before has to be taken into account.

1.6 The QCD phase-diagram

The following figure illustrates the speculative outline of the QCD phase diagram:

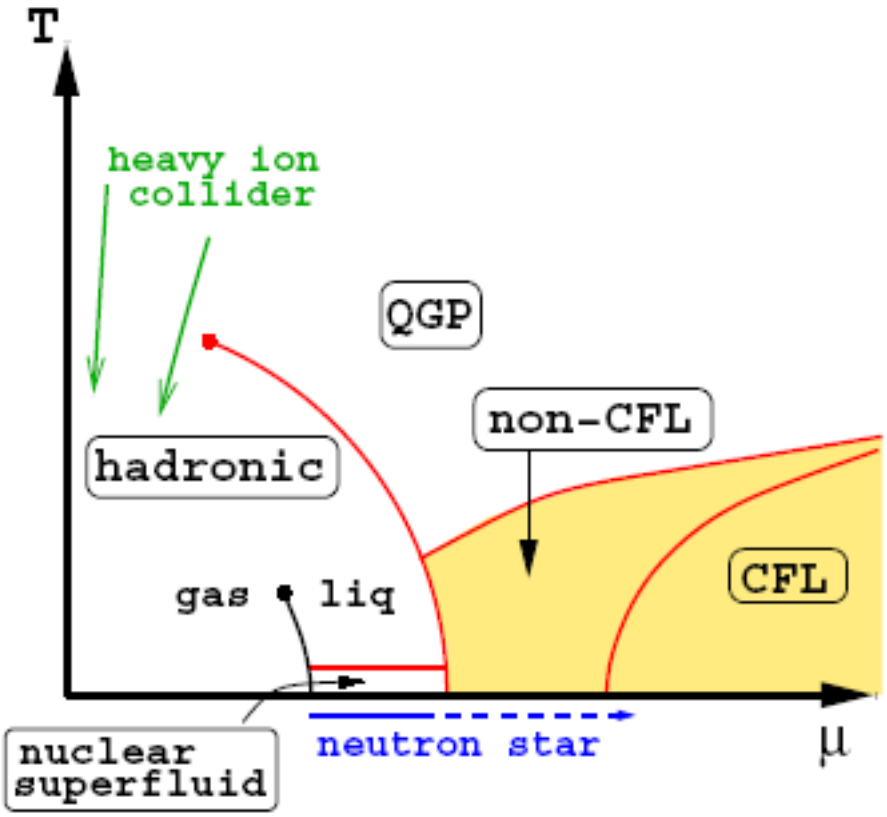

Figure (4): Speculative outline of the QCD phase-diagram taken from reference [13]. The different phases are introduced below. Besides heavy ion collisions, also neutron stars [20] are a valuable test ground for dense matter. An introduction into dense matter in compact stars and observable constraints can be taken for example from reference [9].

Quantum Chromodynamics at finite temperature T and chemical potential μ has a rich phase structure [19]. In principle, in a phase diagram one compares the ground states of all available phases and assigns the one with the lowest energy to the corresponding areas in a T- μ plane. However, in QCD this process is further complicated due to (de)confinement. In many cases, it is crucial to understand whether a phase-transition takes place before or after confinement sets in since some phases explicitly exist only in a confined

or deconfined state. Where exactly this transition line to confinement is located in a T- μ plane , and whether it really is a phase transition is still unknown and subject to intense research. However, reliable results from lattice-QCD predict, that in case of vanishing μ no real phase transition takes place when we move upwards along the T-axis. In other words, a (speculative) phase-transition line separating deconfined quark matter from confined quark matter has to end at a critical point, probably located somewhere near the T-axis. The chiral phase transition in our Ginzburg-Landau calculations also reflects this fact, as we will demonstrate in chapter (2.3). Unfortunately, lattice calculations are limited to regions of very small μ due to a numerical issue referred to as the "sign problem".

In cold low-density matter, a Nambu-Goldstone (NG) phase is realized by breaking of chiral symmetry through condensation of quark-anti-quark pairs whereas for high T these condensates "melt" away and a quark-gluon plasma (QGP) of asymptotically free quarks and gluons is realized. This transition from NG to QGP is currently investigated with the help of ultra-relativistic heavy ion collisions for example at RHIC (Relativistic Heavy Ion Collider) or LHC (Large Hadron Collider). In the case of high μ on the other hand we find color-flavor-locked (CFL) quark matter. This state of matter, in which quarks form cooper pairs and become superconducting can be investigated using first principle (perturbative) calculations since we are in an asymptotically free region of the phase diagram (see section1.5.1). In case of low density nuclear matter on the other hand, a variety of effective theories and sufficient experimental data is available. Hence the most challenging task lies in determining the phase structure in between. Many different approaches to this density region have been pursued. One possibility is to perform calculation within a density regime, that is well under theoretical control and then extrapolate this results up or down to the intermediate density region. Another possibility would be to use an effective model specifically designed to reflect the physical properties of intermediate densities in QCD, such as the NJL model. Our Ginzburg-Landau approach however will be quite different as argued at the beginning of the next chapter.

Besides determining phase transition lines, another interesting question can be investigated within the QCD phase diagram: The fact, that chiral symmetry breaking is also realized in CFL in principle allows for the intriguing possibility of a quark-hadron continuity [21]. Such a continuity is possible if hadronic matter is properly "prepared" by a series of phase transitions, including transitions to hyperonic matter and hyperon superfluids [22]. Looking from the opposite point of view we can start with high density quark matter and study the effect of increasing strange quark masses once we decrease the density. This increase of m_s will impose a stress on the highly symmetric pairing pattern of CFL and it was shown that the first reaction on this stress is the development of a kaon condensate (see section 1.5.4). Also other pairing patterns, which do not break chiral symmetry may occur (in the frame of this work we will consider 2SC). Only if such a phase does not appear before confinement sets in, a smooth quark hadron crossover is possible.

Chapter 2

Phase diagrams in a Ginzburg-Landau model

In the frame of this work, we model the QCD phase structure in a very simplified fashion. The first simplification is the use of a Ginzburg-Landau free energy. We assign specific order parameters to the phases we want to analyze and expand the free energy in terms of these order-parameters up to a certain order. Hence, we have to take into account, that strictly speaking our results are only valid in an area close to second order phase transitions, where the order-parameter is small. The order parameters we are going to consider are a chiral condensate corresponding to the Nambu-Goldstone (NG) phase and a diquark condensate corresponding the the CFL phase, which we later enhance by equipping it with a meson condensate. We will of course not only consider these pure phases but also take into coexistence of both order parameters. Our modeling of the phase structure for increasing chemical potential μ is obviously relatively crude since we have nuclear matter on one hand and CFL matter on the other. Other phases that might appear in between and are necessary to properly "prepare" nuclear matter such, that a smooth quark hadron crossover is possible will not be taken into account in this approach. In this frame, we shall instead ask the question, whether it is possible for the chiral condensate to approach zero smoothly, i.e., without causing an additional phase transition. In [23], it was shown, that this is indeed possible in the case of vanishing strange quark masses. As we shall later argue in more detail, the presence of an $U(1)_A$ violating term (representing the effect of the axial anomaly) which couples diquark and chiral condensates is crucial for the existence of this crossover since it induces a critical point, where a first order transition line, located within the coexistence phase, ends. In the other extreme case of infinite large strange quark mass, we do not find such a critical end point. However, since the real world lies somewhere in between, a first step towards a more realistic phase diagram is to introduce a nonzero but finite strange quark mass, which is demonstrated in chapter (2.3). In the next step, we take into account that CFL breaks chiral symmetry spontaneously, which leads to the octet of pseudo Goldstone-modes, discussed in chapter (1.5.4). As we have shown there, the lightest CFL meson is the neutral kaon, and it was hence suggested, that neutral kaons form a Bose condensate in the presence of a nonzero strange quark mass [16]. The resulting phases have be termed $CFL-K^0$ and $COE-K^0$([24]-[27]) and their interplay with the other phases,taken into account in our Ginzburg-Landau phase diagram will be discussed in chapter (2.4). We should keep in mind however, that by extrapolating down from ultra high densities, meson masses squared are not only represented by a term quadratic in quark masses but also by a linear term which corresponds to the anomaly and is suppressed in the domain of asymptotically large μ . In order words, allowing for $U(1)_A$ violating terms in the Ginzburg-Landau potential, we might have to take into account potentially large corrections to the meson masses and we can only speculate, that the neutral kaon still remains the lightest meson.

The following chapters are organized as follows: We first set up the full Ginzburg-Landau potential including additional mass terms and kaon condensate. Then we review the evaluation of this potential for the case of $m_s = 0$ and vanishing kaon condensate according to [23]. The next step will be to analyze the impact of $m_s \neq 0$ on the phase diagram before we finally "switch on" kaon condensation. At the end of this section we will also discuss the appearance of the 2SC phase due to mass corrections in the Ginzburg-Landau potential.

A few final remarks on the Ginzburg-Landau approach are in order: After this introductionary discussion, one might think that this Ginzburg-Landau approach does not give any "real" answers, since we have to cover an incredibly large (14-dimensional!) parameter space. Within this space, the "real word" lies on a hyper-surface which is recovered by calculating all coefficients in our expansion of the Ginzburg-Landau potential as a function of T and μ. This could be done within an effective theory, such as the NJL model. But looking on this matter from a reversed point of view, we can also state that, by systematically scanning the entire parameter space, we could in principle list all possible scenarios (topologies of the phase diagram). We will however see, that such a systematic scanning is only possible by applying simplifications, which reduce the set of parameters, which have to be taken into account. The great strength of our approach now lies in the model-independence: Any Ginzburg-Landau potential only depends on the symmetries of the phases we want to consider, whereas for example the validity of a NJL calculations depends on validity of the model itself, which is still in dispute. The results we find are thus purely qualitative, but model-independent.

2.1 The Ginzburg-Landau potential

2.1.1 Order parameters

We are interested in a Ginzburg-Landau potential for the chiral and diquark condensates, including a neutral kaon condensate and corrections from the strange quark mass. based on references[23],[28]-[31]. The final result of this section is equation (104), and the following pages are devoted to the derivation of this equation. We shall consider a Ginzburg-Landau free energy of the following form:

$$\Omega = \Omega_\Phi + \Omega_d + \Omega_{\Phi d} \tag{63}$$

with a chiral part Ω_Φ depending only on the chiral condensate Φ, a diquark part depending only on the diquark condensates d_L and d_R (which in turn depend on the kaon condensate) and an interaction part $\Omega_{\Phi d}$ which couples Φ with d_L and d_R. In terms of left- and right-handed quark fields q_L and q_R we have $\left\langle \bar{q}^\alpha_{Ri} q^\alpha_{Lj} \right\rangle \propto \Phi_{ji}$ and $\left\langle q^\alpha_{Li} C q^\beta_{Lj} \right\rangle \propto -\epsilon^{\alpha\beta A}\epsilon_{ijB}[d^+_L]^A_B$, $\left\langle q^\alpha_{Ri} C q^\beta_{Rj} \right\rangle \propto \epsilon^{\alpha\beta A}\epsilon_{ijB}[d^+_R]^A_B$, with flavor indices i, j, B, color indices α, β, A, and the charge conjugation matrix $C = i\gamma^2\gamma^0$ as discussed in section (1.5.2). Since we consider a three-flavor system,Φ, d_L, and d_R are 3×3 matrices.

The quark fields transform under the symmetry group $G \equiv SU(3)_c \times SU(3)_L \times SU(3)_R \times U(1)_B \times U(1)_A$ as:

$$q_L \to e^{i\alpha_B} e^{-i\alpha_A} V_L U \, q_L \tag{64}$$
$$q_R \to e^{i\alpha_B} e^{i\alpha_A} V_R U \, q_R \tag{65}$$

where $(V_L, V_R) \in SU(3)_L \times SU(3)_R$ is a chiral transformation,$U \in SU(3)_c$ is a color gauge transformation, $e^{i\alpha_B} \in U(1)_B$ is a transformation associated with baryon number conservation, and $e^{i\alpha_A} \in U(1)_A$ is an axial transformation. In terms of left- and right-handed $U(1)$ transformations we have $q_L \to e^{i\alpha_L} q_L$, $q_R \to e^{i\alpha_R} q_R$ and the vector and axial $U(1)$ transformations follow from $\alpha_B = (\alpha_R + \alpha_L)/2$, $\alpha_A = (\alpha_R - \alpha_L)/2$, see also section (1.3). Eventually, our potential will not be invariant under the full group G. The chiral group $SU(3)_L \times SU(3)_R$ and the axial $U(1)_A$ become approximate symmetries after including the effects of a small strange quark mass and the QCD axial anomaly, respectively. Since the anomaly breaks $U(1)_A$ down to a discrete subgroup $Z_A(6)$ we will include terms in the potential that are invariant only under $Z_A(6)$, and not under the full $U(1)_A$. We now have to find transformation properties for the order parameters. In case of the chiral condensate, we immediately find:

$$\Phi \to e^{-2i\alpha_A} V_L \Phi V_R^+ \tag{66}$$

In case of the diquark condensate, we have to consider transformations of the (antisymmetric) color and flavor basis, which are given by $[d^A_B]^+ \to (UJ^AU^T)(VI_BV^T)[d^A_B]^+$. The expressions (UJ^AU) and (VI_BV^T) can now be written in terms of matrix multiplications [32]:

$$UJ^AU \to U^+_{Ai} J^i, \qquad VI^BV \to V^+_{Bj} I^j \tag{67}$$

Consequently, we find:

$$[d^A_B]^+ \to U^+_{Ai} J^i V^+_{Bj} I_j [d^A_B]^+ \tag{68}$$
$$[d^A_B] \to [d^A_B](V_{Bj} I_j)(J^i U^T_{iA}) \tag{69}$$

Hence, the full transformation properties of diquark fields are given by:

$$d^A_B \to V d U^T \tag{70}$$

.

More explicitly, in the case of left and right handed diquark fields, we have:

$$d_L \to e^{2i\alpha_B} e^{-2i\alpha_A} V_L d_L U^T \tag{71}$$
$$d_R \to e^{2i\alpha_B} e^{2i\alpha_A} V_R d_R U^T \tag{72}$$

The mass terms are generated by the field

$$M = \begin{pmatrix} m_u & 0 & 0 \\ 0 & m_d & 0 \\ 0 & 0 & m_s \end{pmatrix}, \tag{73}$$

which transforms under G in the same way as the chiral field Φ, $M \to e^{-2i\alpha_A} V_L M V_R^+$. Although we shall write down the Ginzburg-Landau terms with general quark masses m_u, m_d, m_s, we shall later neglect the up and down quark masses and only keep the strange quark mass. Our ansatz for the order parameters is as follows. The chiral field is given by:

$$\Phi = \begin{pmatrix} \sigma_u & 0 & 0 \\ 0 & \sigma_d & 0 \\ 0 & 0 & \sigma_s \end{pmatrix}. \tag{74}$$

We shall derive the potential Ω within this general ansatz, but later set for simplicity $\sigma_u = \sigma_d = \sigma_s$. Different values for each quark flavor are more realistic in the presence of a strange quark mass and a kaon condensate. However, this would introduce additional independent parameters into our potential, making a systematic evaluation very complicated. Therefore, we shall use the symmetric case as a simplification.

For the diquark condensate and the diquark chiral field we use the ansatz discussed in chapter (1.5.4):

$$d_L = d_R^\dagger = d \begin{pmatrix} 1 & 0 & 0 \\ 0 & \cos(\phi/2) & i\sin(\phi/2) \\ 0 & i\sin(\phi/2) & \cos(\phi/2) \end{pmatrix}, \qquad \Sigma = \frac{d_L d_R^+}{d^2} \begin{pmatrix} 1 & 0 & 0 \\ 0 & \cos\phi & i\sin\phi \\ 0 & i\sin\phi & \cos\phi \end{pmatrix} \tag{75}$$

where ϕ is the kaon condensate. For $\phi = 0$ we recover the pure CFL order parameter $d_L = d_R = \mathrm{diag}(d, d, d)$. Note however, that while d_L and d_R are gauge variant quantities, Σ is gauge invariant. Therefore, our ansatz is one of infinitely many choices for d_L and d_R - all related by gauge transformations. The field Σ transforms under G as:

$$d_L d_R^\dagger \to e^{-4i\alpha_A} V_L d_L d_R^\dagger V_R^+ . \tag{76}$$

This is the same transformation property as the ordinary chiral field Φ, except for the transformations under $U(1)_A$. This difference reflects the fact that in CFL the mesons are composed of four quarks, not two.

2.1.2 Chiral potential

We can now derive the explicit form of the potential Ω and we start with the chiral part Ω_Φ . We collect all terms up to fourth combined order in M and Φ with at most one power in the mass field M. The terms of $\mathcal{O}(M^0)$ which are invariant under G are:

$$\mathrm{Tr}[\Phi^+\Phi] = \sigma_u^2 + \sigma_d^2 + \sigma_s^2 \tag{77}$$
$$(\mathrm{Tr}[\Phi^+\Phi])^2 = (\sigma_u^2 + \sigma_d^2 + \sigma_s^2)^2 \tag{78}$$
$$\mathrm{Tr}[(\Phi^+\Phi)^2] = \sigma_u^4 + \sigma_d^4 + \sigma_s^4 \tag{79}$$

If we do not require the potential to be invariant under $U(1)_A$, we have the additional term [34]:

$$\det\Phi + \text{h.c.} \propto \epsilon_{abc}\epsilon_{ijk}\Phi_{ai}\Phi_{bj}\Phi_{ck} + \text{h.c.} = 12\sigma_u\sigma_d\sigma_s \tag{80}$$

Because of $\det\Phi \to e^{-6i\alpha_A}\det\Phi$, this term is only invariant under the discrete subgroup $Z_A(6) \subset U(1)_A$, as expected from the anomaly. Microscopically, $\det\Phi$ accounts for an effective six-point instanton vertex which converts three left-handed quarks into three right-handed quarks, thus violating axial charge conservation by an amount $2N_f = 6$.

The terms of order $\mathcal{O}(M^1)$ arise from replacing one chiral field Φ by the mass field M in each of the above $\mathcal{O}(M^0)$ terms. We obtain:

$$\mathrm{Tr}[M\Phi^+] + h.c. = 2(m_u\sigma_u + m_d\sigma_d + m_s\sigma_s) \tag{81}$$
$$\mathrm{Tr}[M\Phi^+]\mathrm{Tr}[\Phi\Phi^+] + h.c. = 2(m_u\sigma_u + m_d\sigma_d + m_s\sigma_s)(\sigma_u^2 + \sigma_d^2 + \sigma_s^2) \tag{82}$$
$$\mathrm{Tr}[M\Phi\Phi^+\Phi] + h.c. = 2(m_u\sigma_u^3 + m_d\sigma_d^3 + m_s\sigma_s^3) \tag{83}$$
$$\epsilon_{ijk}\epsilon_{abc}M_{ai}\Phi_{bj}\Phi_{ck} + h.c. = 4(\sigma_u\sigma_d m_s + \sigma_u\sigma_s m_d + \sigma_d\sigma_s m_u) \tag{84}$$

We can now add all these contributions, each coming with a separate prefactor and obtain the chiral potential. Approximating $m_u \simeq m_d \simeq 0$ and setting for simplicity $\sigma_u = \sigma_d = \sigma_s \equiv \sigma$, we can write the potential as

$$\Omega_\Phi = a_0 m_s\sigma + \frac{a_1 + m_s a_2}{2}\sigma^2 + \frac{c_1 + m_s c_2}{3}\sigma^3 + \frac{b}{4}\sigma^4\,. \tag{85}$$

In the given approximation, m_s gives rise to a linear term in σ and yields corrections to the quadratic and cubic terms. Because of the linear term, the chiral condensate cannot vanish exactly in the ground state. Instead of a vacuum phase with $\sigma = 0$ there will be a phase with very small σ where chiral symmetry is approximately restored and which is continuously connected to the chirally broken phase in which σ has a sizable value. This is the most obvious consequence of the mass term. Due to the coupling of chiral and diquark condensates, to be discussed in section (2.1.4), we shall find other, less obvious, effects of the linear term for our phase diagram. These effects are discussed in section (2.3)

2.1.3 Diquark potential

For the diquark potential Ω_d we also start from the terms up to $\mathcal{O}(d^4)$, first without mass insertions. Within our CFL-K^0 ansatz they simply yield the structures d^2 and d^4 since the kaon condensate always drops out:

$$\mathrm{Tr}[d_L d_L^+] = \mathrm{Tr}[d_R d_R^+] = 3d^2 \tag{86}$$
$$(\mathrm{Tr}[d_L d_L^+])^2 = (\mathrm{Tr}[d_R d_R^+])^2 = (\mathrm{Tr}[d_L d_L^+])(\mathrm{Tr}[d_R d_R^+]) = 9d^4 \tag{87}$$
$$\mathrm{Tr}[(d_L d_L^+)^2] = \mathrm{Tr}[(d_R d_R^+)^2] = \mathrm{Tr}[(d_R d_L^+ d_L d_R^+] = 3d^4 \tag{88}$$

All these terms are invariant under the full group G. There is no such term as $\det d_{L,R}$ since this term would not only break $U(1)_A$ but also baryon number conservation which must not be explicitly broken. To include the effect of quark masses, we need to replace $d_L d_R^+$ by M. From the above equations, the only possible term (except for a term constant in d_L, d_R which we can omit) is

$$\mathrm{Tr}[d_L^+ M d_R] + \mathrm{h.c.} = 2d^2[m_u + (m_d + m_s)\cos\phi]\,. \tag{89}$$

This term is invariant under $Z_A(6) \subset U(1)_A$ and thus is allowed in the presence of the anomaly. Other $\mathcal{O}(M^1)$ terms arise from replacing one chiral field $d_L d_R^+$ in the $\mathcal{O}(d^6)$ terms. They all yield the same structure and are invariant under $Z_A(6)$:

$$\mathrm{Tr}[d_L^+ M d_R d_R^+ d_R] + \mathrm{h.c.} = 2d^4\,[m_u + (m_d + m_s)\cos\phi] \tag{90}$$
$$\mathrm{Tr}[d_L^+ M d_R d_L^+ d_L] + \mathrm{h.c.} = 2d^4\,[m_u + (m_d + m_s)\cos\phi] \tag{91}$$
$$\mathrm{Tr}[d_L^+ M d_R]\mathrm{Tr}[d_R^+ d_R] + \mathrm{h.c.} = 6d^4\,[m_u + (m_d + m_s)\cos\phi] \tag{92}$$
$$\mathrm{Tr}[d_L^+ M d_R]\mathrm{Tr}[d_L^+ d_L] + \mathrm{h.c.} = 6d^4\,[m_u + (m_d + m_s)\cos\phi] \tag{93}$$

So far the only structure we have produced for the kaon condensate is $\cos\phi$. If we were to stop here, the minimization of Ω_d would not allow for nontrivial condensates. This would be in contradiction to high-density calculations. Therefore we need to include at least one extra term with nontrivial structure in ϕ.

To find the term providing this non trivial structure, we turn to the discussion of the high density effective theory in section (1.5.5). We first notice, that the term linear in the masses in the effective Lagrangian (57) corresponds to the term (89) introduced above. However, the kaon mass, given by equation (62) also includes a term quadratic in the quark masses (which is dominant in high density regions), which we will not cover in our potential since it wont reproduce the desired non-trivial structure in ϕ. Including terms coming from the covariant derivatives (59), we find a non trivial contribution $\propto \mu^2 sin^2\phi$ which also contains the square kaon chemical potential (62) and hence is of the order $O(M^4)$. This term is crucial for kaon condensation to occur as one can check by expanding $V(\phi)$ in equation (60) up to the order of ϕ^4 to reproduce the potential of an ordinary ϕ^4- model. The resulting ϕ^2 term becomes negative only for $\mu > m_{K^0}$ in which case a nonzero value of ϕ minimizes the potential. We thus conclude that the critical strange quark mass for the onset of kaon condensation scales at high density as $m_s \sim m_u^{1/3}\Delta^{2/3}$. At this point, it might seem inconsistent to drop terms quadratic in the mass but keep terms $O(M^4)$. We justify this by arguing, that this term can become comparable to the $O(M^2)$ terms [16] and introduces a qualitatively new structure to our Ginzburg-Landau potential. In other words, terms $O(M^2)$ would simply provide corrections to the Ginzburg-Landau coefficients $\propto d^2$ and $\propto d^4$(which will not introduce any qualitative changes in the phase diagram as we shall argue later). We hence include the following term:

$$\mathrm{Tr}[[MM^+, d_L d_R^+][M^+M, d_R d_L^+]] = -2d^4(m_d^2 - m_s^2)^2 \sin^2\phi\,. \tag{94}$$

and assume -guided by the high density results- that the coefficient in front of this term is large enough to compensate for the suppression of the quark masses.

We can now collect all diquark terms and set $m_u \simeq m_d \simeq 0$ to write the diquark potential as

$$\Omega_d = \frac{\alpha_1 + \alpha_2 m_s \cos\phi}{2}\, d^2 + \frac{\beta_1 + \beta_2 m_s \cos\phi - \mu^2 \sin^2\phi}{4}\, d^4\,, \tag{95}$$

where we have written the prefactor of the term $\propto sin^2\phi$ as μ^2, reminiscent of the effective kaon chemical potential of the effective theory.

2.1.4 Interaction potential

For the interaction potential $\Omega_{\Phi d}$, the term of lowest order in the order parameters is

$$\mathrm{Tr}[d_R d_L^+ \Phi] + \text{h.c.} = 2d^2[\sigma_u + (\sigma_d + \sigma_s)\cos\phi]\,. \tag{96}$$

This term is anomalous since it is not invariant under $U(1)_A$. Without kaon condensate it has already been considered in [23]. We see that, in contrast to the pure diquark terms, the kaon condensate appears even in the absence of a strange quark mass. Including one more power in Φ yields the following terms which are invariant under the full symmetry group G:

$$\mathrm{Tr}[d_L d_L^+ \Phi\Phi^+] = \mathrm{Tr}[d_R d_R^+ \Phi\Phi^+] = d^2(\sigma_u^2 + \sigma_d^2 + \sigma_s^2) \tag{97}$$

$$\mathrm{Tr}[d_L d_L^+ + d_R d_R^+]\mathrm{Tr}[\Phi^+\Phi] = d^2(\sigma_u^2 + \sigma_d^2 + \sigma_s^2) \tag{98}$$

$$Det\Phi\,\mathrm{Tr}[d_L d_R^+ \Phi^{-1}] + h.c. = 2[\sigma_d\sigma_s + \sigma_u(\sigma_d + \sigma_s)cos\phi] \tag{99}$$

We include mass terms up to $\mathcal{O}(M^1)$, which arise from replacing a chiral field Φ in the above expressions (obviously, replacing a field $d_L d_R^+$ in these terms does not yield interaction terms):

$$\mathrm{Tr}[d_L d_L^+ M\Phi] + h.c. = 2d^2(m_u\sigma_u + m_d\sigma_d + m_s\sigma_s) \tag{100}$$

$$\mathrm{Tr}[d_L d_L^+ + d_R d_R^+]\mathrm{Tr}[M^+\Phi] + h.c. = 12d^2(m_u\sigma_u + m_d\sigma_d + m_s\sigma_s) \tag{101}$$

$$\epsilon_{abc}\epsilon_{ijk} M_{ai}\Phi_{bj}(d_L d_R^+)_{ck} = 2d^2\{m_d\sigma_s + m_s\sigma_d + [m_u(\sigma_d + \sigma_s) + \sigma_u(m_d + m_s)]\cos\phi\} \tag{102}$$

Estimates of the prefactor of the $d^2\sigma^2$ term suggest this contribution to be negligible [23]. We shall thus focus only on the $d^2\sigma$ terms, as it was done for the three-flavor case in reference [23]. Then, collecting the

terms and again setting $m_u \simeq m_d \simeq 0$, $\sigma_u = \sigma_d = \sigma_s \equiv \sigma$, the most general form of the interaction potential can be written as

$$\Omega_{\Phi d} = -\left[\gamma \frac{1+2\cos\phi}{3} + m_s(\gamma_1 + \gamma_2 \cos\phi)\right] d^2\sigma \tag{103}$$

For $\phi = m_s = 0$ we recover the interaction term $-\gamma d^2\sigma$ from reference [23].

2.1.5 Complete Potential

We can now put the contributions of sections (2.1.2-2.1.4) together to obtain the full Ginzburg-Landau potential, including mass corrections and the meson condensate in the approximations discussed above,

$$\begin{aligned}\Omega = a_0 m_s \sigma + \frac{a_1 + m_s a_2}{2}\sigma^2 + \frac{c_1 + m_s c_2}{3}\sigma^3 + \frac{b}{4}\sigma^4 \\ + \frac{\alpha_1 + \alpha_2 m_s \cos\phi}{2} d^2 + \frac{\beta_1 + \beta_2 m_s \cos\phi - \mu^2 \sin^2\phi}{4} d^4 \\ - \left[\gamma \frac{1+2\cos\phi}{3} + m_s(\gamma_1 + \gamma_2\cos\phi)\right] d^2\sigma\end{aligned} \tag{104}$$

Equipped with this Potential, we will now try to systematically analyze the phase structure resulting from the interplay between chiral and diquark condensates including the effects of axial anomaly, strange quark mass and kaon condensation. The dynamics of this interplay are given by the stationary equations:

$$\frac{\partial\Omega}{\partial\sigma} = \frac{\partial\Omega}{\partial d} = \frac{\partial\Omega}{\partial\phi} = 0 \tag{105}$$

As written in the full potential (104), there are 14 independent parameters. This is too unwieldy for a systematic study and therefore we shall work in several limit cases in the subsequent sections. In the next section we start with the case of a vanishing quark masses and kaon condensate. We are reproducing the results from reference [23], which can be considered the ground work for all our advanced studies.

2.2 Vanishing quark masses and meson condensate.

In the limit case of vanishing quark masses and meson condensate, we have to consider the following potential:

$$\Omega(\sigma, d) = \frac{a}{2}\sigma^2 - \frac{c}{3}\sigma^3 + \frac{b}{4}\sigma^4 + \frac{\alpha}{2}d^2 + \frac{\beta}{4}d^4 - \gamma d^2\sigma\,. \tag{106}$$

Note, that a term linear in σ is proportional to m_s and hence vanishes completely for $m_s = 0$. Changes in the sign of a and α drive the phase transitions. We shall hence use these variables as key parameters (axes of the phase diagram). Before going into the details of the evaluation of the phase structure, we review constraints on the parameters of equation (106) provided in reference [23]. We shall also rely on these constraints through the remainder of this chapter.

- We assume b to be positive. However, b may change sign as a function of T and μ in which case the above potential would become unstable. We are then forced to introduce a term proportional to σ^6 and an additional coefficient $f > 0$, but qualitative phase structure of three massless flavors is not influenced by this.
- we assume β to be always positive as expected from effective theories and weak coupling QCD
- terms $\propto d^2\sigma$ as well as $\propto \sigma^3$ are both originating from the axial anomaly. Their corresponding coefficients c and γ are microscopically related. In particular, they come with the same sign and order of magnitude. The coefficients c and γ are then both considered positive.

With these conditions in mind, we can now minimize the potential and ask for the corresponding ground state. We now have to distinguish between four possible cases:

1. Normal (NOR) phase: $\sigma = 0$ and $d = 0$. The only phase completely invariant under the group G which physically corresponds to Quark-Gluon Plasma (QGP).
2. CSC phase: $\sigma = 0$ but $d \neq 0$. Pure CFL color superconductor. Looking at equation (106) we find, that it is impossible to realize $d \neq 0$ if $\sigma = 0$ and CFL is only approximately realized.
3. NG phase: $d = 0$ but $\sigma \neq 0$.
4. Coexistence (COE) phase: $\sigma \neq 0$ and $d \neq 0$. A color superconductor on the CFL phase with non vanishing chiral condensate.

The stationary equations are:

$$\frac{\partial\Omega}{\partial d} = 2d(\frac{\alpha}{2} + \frac{\beta}{2}d^2 - \gamma\sigma) = 0 \tag{107}$$

$$\frac{\partial\Omega}{\partial\sigma} = a\sigma - c\sigma^2 + b\sigma^3 - \gamma d^2 = 0 \tag{108}$$

For the determination of the ground state it is useful to also consider the second derivatives. The Hessian matrix of $\Omega(d, \sigma)$ is

$$H = \begin{pmatrix} \frac{\partial^2\Omega}{\partial\sigma^2} & \frac{\partial^2\Omega}{\partial\sigma\partial d} \\ \frac{\partial^2\Omega}{\partial d\partial\sigma} & \frac{\partial^2\Omega}{\partial d^2} \end{pmatrix} = \begin{pmatrix} a - 2c\sigma + 3b\sigma^2 & -2\gamma d \\ -2\gamma d & \alpha + 3\beta d^2 - 2\gamma\sigma \end{pmatrix}. \tag{109}$$

For a solution to be a local minimum, the Hessian, evaluated at this solution, must have positive eigenvalues. If the potential is bounded from below – which is guaranteed by $b, \beta > 0$ – the solution with the lowest free energy yields the ground state, i.e., the global minimum, unambiguously. In other words, if we find a stationary point of the potential with a negative eigenvalue of its Hessian, then we must also have found another stationary point with lower free energy. Since the potential is bounded from below, the stationary point with lowest free energy must have a positive definite Hessian. Consequently, the second derivatives are strictly speaking not necessary for a stability check. We shall however, use them to determine phase transition lines in a relatively simple way by using the eigenvalues of the Hessian (see appendix [2]).

2.2.1 Nambu Goldstone phase

In the case of the Nambu Goldstone phase, the first stationary equation (107) is automatically fulfilled since d=0. The second equation yields

$$\sigma = \frac{c}{2b} \pm \sqrt{\frac{c^2}{4b^2} - a}, \qquad \sigma = 0 \tag{110}$$

$\sigma = 0$ leads to the normal phase and is not of any interest right now. We can now use the stability criterion of the Hessian discussed above. The Hessian in the case of a vanishing diquark condensate is given by:

$$H(d=0) = \begin{pmatrix} a - 2c\sigma + 3b\sigma^2 & 0 \\ 0 & \alpha - 2\gamma\sigma \end{pmatrix} \tag{111}$$

leading to the following set of conditions for a and α:

$$a > 2c\sigma + 3b\sigma^2 \tag{112}$$

$$\alpha > 2\gamma\sigma \tag{113}$$

We can use the second inequality to find a phase transition line exactly when $\alpha = 2\gamma\sigma(a)_{min}$ where $\sigma(a)_{min}$ is given by equation (110). The two possible solutions then are:

$$\alpha = \frac{\gamma}{b}(c \pm \sqrt{c^2 - 4ba}) \tag{114}$$

Additionally using (112) we can restrict ourselves to the positive sign in (114). We will review all phase transition in terms of symmetries in chapter (2.2.3). Next we turn to the transition between NG and NOR phase. Here we can make use of the fact, that the coupling γ is irrelevant, since d vanishes in both phases. We then demand $\Omega_{NG} = \Omega_{NOR} = 0$ at the potential minimum and find:

$$a = \frac{2c^2}{9b} \tag{115}$$

2.2.2 Coexistence and approximate CFL phase

It remains to determine interplay of the COE and the (approximate) CFL phase as well as transition between the COE and the NOR phase. The latter is the hardest task and the transition line can partially only be determined by a numerical approach. For more details on numerics, refer to appendix 2. First, we express $\sigma = \sigma(d)$ and find:

$$\Omega^{Coe}(\sigma(d), d) = \Omega_0 + \frac{\alpha^*}{2}d^2 + \frac{\beta^*}{4}d^4 \tag{116}$$

where just as in the opposite case before, α^* and $\beta^*$are expressions of the old parameters set $\alpha, \beta, \gamma, a, b, c$. This expression is equivalent to the potential of an Ising ferromagnet in case of $\beta^* > 0$. We are especially interested in the explicit form of the coefficient α^* , since changes in this coefficient lead to a phase transition in case of the given potential (116):

$$\alpha^* = \frac{\beta\alpha}{32\gamma^6}(4b\gamma^2\alpha^2 - 8c\alpha\gamma^3 + 16a\gamma^4) \tag{117}$$

At the same time,β^*, given by $\beta^* = \frac{\beta}{32\gamma^6}(12b\gamma^2\alpha^2 - 16c\gamma^3\alpha + 16a\gamma^4 - 32\frac{\gamma^6}{\beta}$ must not be negative. The condition $\alpha^* = 0$ obviously also implies $\alpha = 0$ which partly represents the phase transition line to the NOR

phase we were looking for. The remaining two solutions for α in (117) lead back to the solutions (110) we have already obtained. However, one difficulty here is given by the fact that in case of the COE phase, both condensates have to coexist at the same time, and hence we have an additional constraint $d(\sigma) \ \epsilon \ \mathbb{R}$. This condition sets in at the borderline between COE and NOR phase and we hence have to numerically ask, which phase represents the ground state in agreement with this additional constraint. We find, that the straight line of the first order phase transition in the COE phase (see text below and figure 7) terminates at the intersection with the second-order line and then continues as a nontrivial, non-straight, curve.

For the analysis of the inner structure of the coexistence phase, we eliminate d in equation (107) instead of σ which yields $d = 0$ or $d^2 = (\frac{2}{\beta})(\gamma\sigma - \frac{\alpha}{2})$. Inserting the $d \neq 0$ solution into the potential, we find:

$$\Omega^{COE}(\sigma, d(\sigma)) = -\frac{\alpha^2}{4\beta} + \gamma^*\sigma + \frac{a^*}{2}\sigma^2 - \frac{c}{3}\sigma^3 + \frac{b}{4}\sigma^4 \tag{118}$$

where we have abbreviated:

$$\gamma^* = \frac{\alpha\gamma}{\beta}, \qquad a^* = a - 2\frac{\gamma^2}{\beta} \tag{119}$$

Solving for the stationary equation $\frac{\partial\Omega}{\partial\sigma} = 0$ now involves solving a cubic equation in σ . Although this can in principle be done analytically, it is very hard to extract information out of these lengthy solutions. Solutions to cubic equations will play a key role also in the following sections. We shall therefore follow two approaches:

- we introduce a linear shift to the σ fields by setting $\sigma \to \tau = \sigma - \frac{c}{(3b)}$. This will not only eliminate the σ^3 term but also allow for some important analytical observations such as the existence of a critical point as we will demonstrate below.
- we will numerically produce phase diagrams in order to gain information even from those regions, which are to complicated to be treated analytically. The agreement of our analytical and numerical results provides a valuable check of both approaches (Appendix [2])

The shifting of the fields in σ results in a new form of the potential:

$$\Omega^{COE}(\tau) = \Omega_c + \gamma_c^*\tau + \frac{a_c^*}{2}\tau^2 + \frac{b}{4}\tau^4 \tag{120}$$

with:

$$\Omega_c = -\frac{\beta}{4\gamma^2}\gamma^{*2} + \frac{c}{3b}\gamma^* + \frac{c^2}{18b^2}a^* - \frac{c^4}{108b^3} \tag{121}$$

$$\gamma_c^* = \gamma^* + \frac{c}{3b}a^* - \frac{2c^3}{27b^2} \tag{122}$$

$$a_c^* = a^* - \frac{c^2}{3b} \tag{123}$$

We again exploit the analogy to solid state physics, where an equivalent system is given by an Ising ferromagnet in an external magnetic field. We therefore expect the existence of a critical point at which a first order phase transition line ends, just as in the case of ferromagnetism. In order to understand this phenomenon, we consider figure(5) below. We have divided the entire phase space into regions where the linear or the quadratic term is smaller or bigger than zero. By looking at the shape of the potential $\Omega(\tau)$ we find that by crossing the line at which the linear term vanishes, the order parameter τ jumps discontinuously between $\tau = \pm\sqrt{\frac{-a_c^*}{b}}$. However, if we also happen to cross the line at which the quadratic term in τ vanishes, we see that there is no more jump of the order parameter but a smooth transition. Hence we find cross-over instead of a real phase transition for this region. Qualitatively, the existence of such a critical point can be understood in terms of residual symmetries, determined by the effect of the axial anomaly. We will discuss this issue in more detail in the next section.

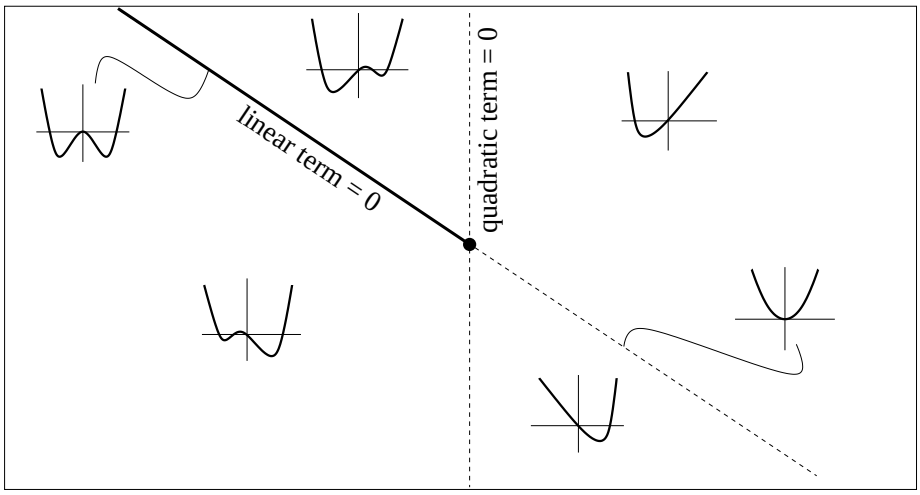

Figure (5): Illustration of the appearance of a critical point for a free energy with a linear, quadratic, and positive quartic term in the order parameter, such as in equation (120). The coefficients in front of the linear and the quadratic term change their sign across the two straight lines. For a negative quadratic term there is a first-order phase transition, indicated by the thick solid line. This line ends at the critical point at which both linear and quadratic terms vanish. Across the dashed lines there is no phase transition. This implies that one can smoothly connect two nontrivial minima of the potential by "going around" the first order line. In our context, these two phases are the COE phase and the (approximate) CFL phase.

Setting $\gamma_c^* = a_c^* = 0$, we find the position of the critical point in our $a - \alpha$ plane:

$$P_c = (\frac{c^2}{3b} + \frac{2\gamma^2}{\beta}, -\frac{\beta c^3}{27\gamma b^2}) \tag{124}$$

and the first order line, determined by $\gamma_c^* = 0$ is given by:

$$\alpha = -\frac{\beta c}{3\gamma b}a + \frac{2\gamma c}{3b} + \frac{2\beta c^3}{27\gamma b^2} \tag{125}$$

This situation is illustrated in figure (6):

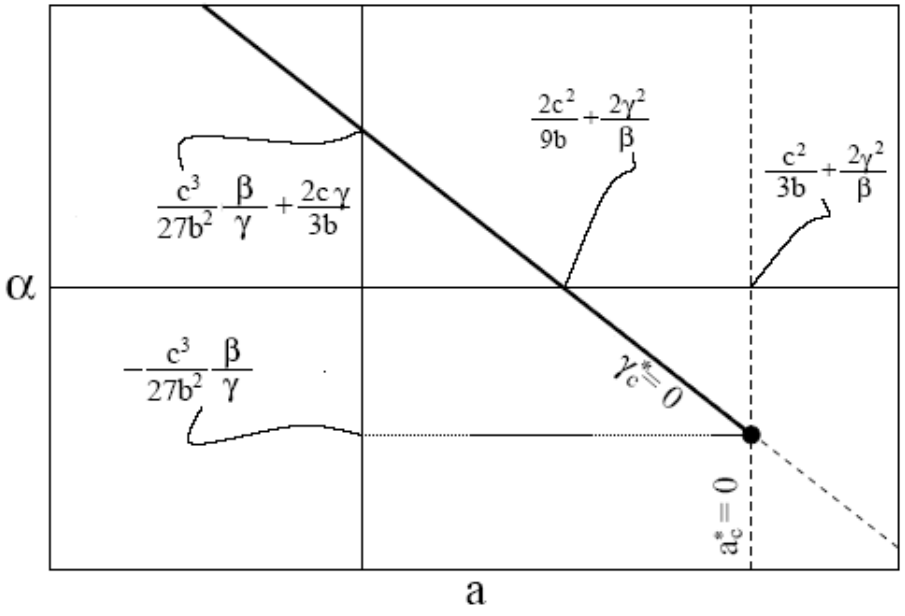

Figure(6): first order phase transition line (thick solid line) and critical point in the (a, α) plane within the COE phase. This critical point in the COE phase is present only due to instanton effects and vanishes from the phase diagram for $\gamma = 0$, as we shall explain below.

It is obvious that the critical point is a consequence of the anomaly: if the anomalous term vanishes,$\gamma = 0$, the critical point disappears from the phase diagram because its α coordinate goes to $-\infty$ or $+\infty$, depending on the sign of $\frac{c^3}{27b^2}$ (while its a coordinate remains finite). This leaves a first order phase transition between the COE and the CFL phase, while for $\gamma > 0$ there is a crossover between the COE and the approximate CFL phase. We shall discuss both scenarios in terms of symmetries in the next section and end this one by summarizing all analytical and numerical results of the previous two sections in figure (7):

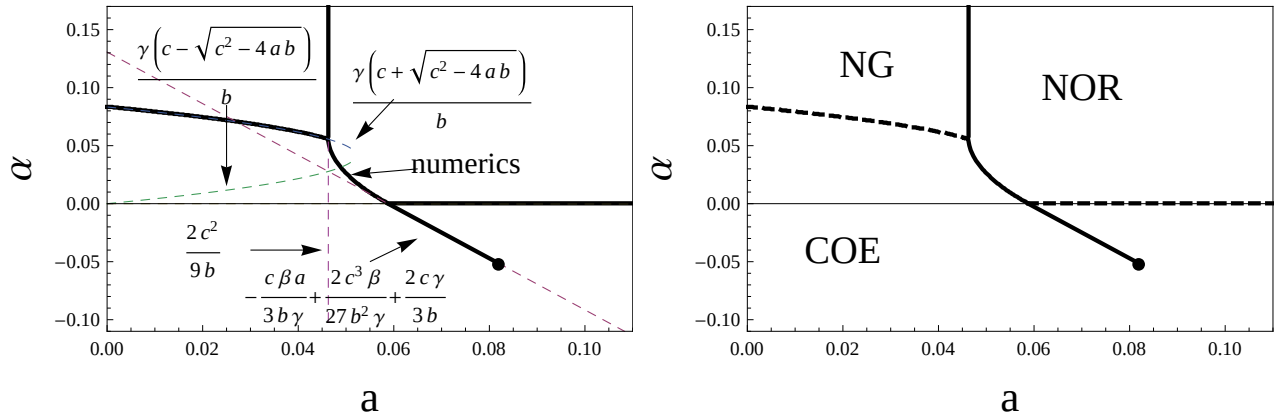

Figure(7):Left panel: Analytical curves and shape of the resulting phase diagram (thick black lines). The only region, which cannot be determined by analytical means is located in between the $\alpha = 0$ and $\alpha = \frac{\gamma}{b}(c + \sqrt{c^2 - 4ba})$. From our analytical analysis, one could have expected the straight first-order line to be present wherever the $\gamma_c^* = 0$ line lives in the COE region. The reason for this different behavior is the condition $d \in \mathbb{R}$. In terms of the schematic potentials of figure (5), the first order line separates two nontrivial minima. Here, for positive α, the second minimum is forbidden since it would imply $d^2 < 0$. Consequently, upon crossing the line $\gamma_c^* = 0$ the ground state remains in the same local minimum although, if one had ignored the condition $d^2 > 0$, there would have be a second local minimum with lower free energy. Right panel: Phase diagram and corresponding phases. Here the dashed lines represent second order transitions, whereas a thick black lines represents a first order transition. In order to simplify our diagrams, we will not include analytical lines in the following chapters but refer to the discussion in the Appendix [A2].

2.2.3 Symmetries of the phase diagram

Before we extend our model by including effects of the strange quark mass and meson condensation, we review the last chapter and try to gain a deeper qualitative insight by analyzing the symmetries of all phases involved. In figure (8),we compare two different scenarios: One where we set the coefficient γ equal to zero, and one where we leave it non-zero. Since γ corresponds to the only interaction term in our approximation, the chiral and diquark parts of the free energy decouple, resulting in a very simple phase diagram (left panel). In this phase diagram COE and CFL phases are separated by a first order line which does not end at a critical point (vertical solid line).

As indicated in figure(8), the symmetries of COE and CFL are different without the anomaly. In other words, adding a chiral condensate to the CFL phase changes the (discrete) symmetries of the phase. This can be seen from the transformation properties of the order parameters in equations (66) and (67). The chiral condensate $\Phi = \mathrm{diag}(\sigma, \sigma, \sigma)$ and the CFL diquark condensate spontaneously break the chiral group $SU(3)_L \otimes SU(3)_R$ down to the vector subgroup of simultaneous left- and right-handed rotations $SU(3)_V$. From equation (66) we see, that any chiral condensate is also invariant under $U(1)_B$ transformations and under transformations of an axial subgroup $\mathbb{Z}_A(2)$. However, this $\mathbb{Z}_A(2)$ is contained in $U(1)_B$. To see this it is helpful to consider the group $U(1)_L \otimes U(1)_R$ as a topological space, in this case a torus, on which the discrete subgroups are sets of discrete points. We show this geometric picture in figure(9), which illustrates and facilitates the discussion of the discrete subgroups, in particular since we switch repeatedly between the bases of left- and right-handed rotations vs. axial and vector rotations, which can be confusing without this illustration.

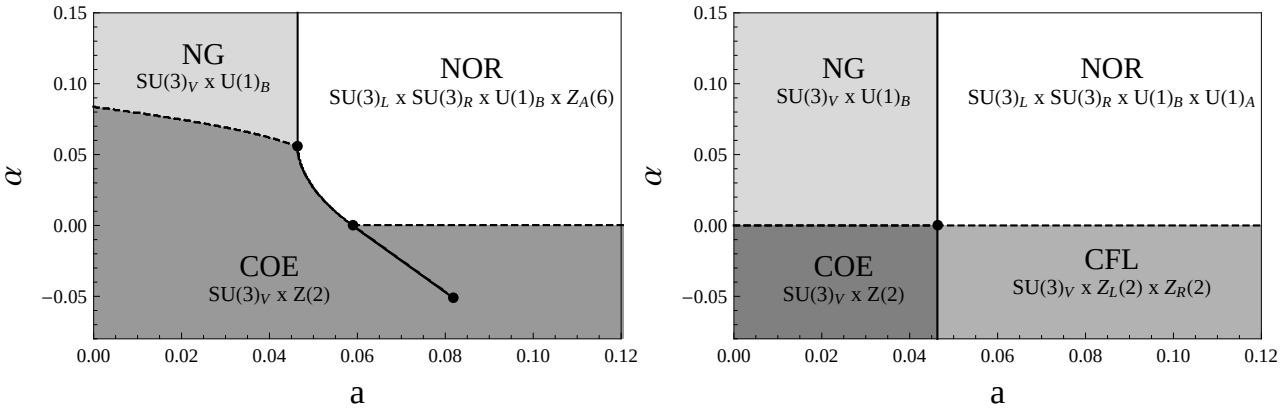

Figure (8): Phase diagrams in the (a, α) plane without strange quark mass effects and without meson condensation, without (left panel) and with (right panel) anomalous effects. First-order phase transition lines are solid, second-order lines are dashed. For each phase we have indicated its global symmetries. They explain why the first-order phase transition line does not (left) and does (right) end at a critical point (see below for a detailed discussion). The vertical (first-order) phase transition line separating NG from NOR (left and right) and COE from CFL (left) is located at $a = 2c^2/(9b)$. We have set the Ginzburg-Landau parameters to $b = 1.2$, $c = 0.5$, $\beta = 1.6$ for both plots, and $\gamma = 0$ (left), $\gamma = 0.1$ (right). This particular choice is completely irrelevant for the topology of the left plot. For the right plot, one slightly different topology can be obtained in a different class of parameter values, where the phase transition between NG and COE is of first order along a certain piece of the transition line, see right panel of Fig. 2 in reference [23].

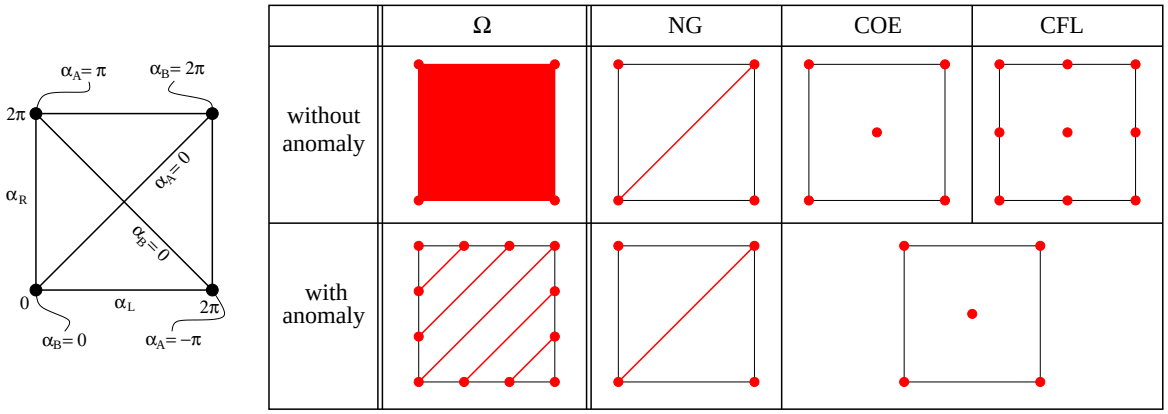

Figure (9): Diagram (left): topological space of $U(1)_L \otimes U(1)_R$ with generators $\alpha_L, \alpha_R \in [0, 2\pi]$. Opposite sides of the square have to be identified (in particular, all four corners of the square correspond to the unit element). The resulting torus can also be parametrized by $\alpha_B = (\alpha_R + \alpha_L)/2 \in [0, 2\pi]$ and $\alpha_A = (\alpha_R - \alpha_L)/2 \in [-\pi, \pi]$. Table (right): symmetries of the free energy Ω and the NG, COE, and CFL phases without and with axial anomaly. Thick (red) lines and points indicate group elements under which the free energy and the respective phases are invariant. For instance, in the first row, the points for the COE phase are obtained as the common subset of the points of the NG and CFL phases (and all sets of points are subsets of the points for Ω). Only with anomaly, i.e., only after restricting the symmetry of Ω from $U(1)_L \otimes U(1)_R$ to $U(1)_B \times Z_A(6)$, the symmetries of COE and CFL are identical, allowing for a smooth crossover between these two phases.

In contrast to the chiral condensate, the diquark condensates d_L, d_R break $U(1)_B$ spontaneously. Hence there must be a true phase transition separating the NG and NOR phases from the COE and CFL phases. This statement is independent of the anomaly. The anomaly becomes important for the difference between COE and CFL phases. In the absence of instanton effects, the diquark condensates are invariant under independent sign flips of left- and right-handed quark fields, $Z_L(2) \otimes Z_R(2)$. This discrete group is broken by the chiral condensate; therefore, the COE phase, containing both order parameters, is only invariant under the common subgroup of $U(1)_B$ and $Z_L(2) \otimes Z_R(2)$. This is the group of simultaneous sign flips, $Z(2)$. As a result, without axial anomaly COE and CFL have different residual symmetry groups, see first row of the table in figure (9).

The anomaly reduces the axial symmetry $U(1)_A$ of the potential to $Z_A(6)$, see figure 1. The group $U(1)_B \times Z_A(6)$ is represented in the first panel of the second row in figure (9). The anomaly does not affect the residual group of the NG phase. However, the residual group of the CFL phase is reduced since only $Z(2) \subset Z_L(2) \times Z_R(2)$, not the entire group $Z_L(2) \otimes Z_R(2)$, is a subgroup of $U(1)_B \times Z_A(6)$, as can be seen geometrically in figure (9) . Therefore, if instanton effects are taken into account, CFL is invariant only under the group of simultaneous sign flips $Z(2)$. Now the addition of the chiral condensate does not further reduce this group, and the residual groups of COE and CFL become identical, see second row of figure (9). This allows for a smooth crossover between these two phases, and thus the first-order line between COE and (approximate) CFL can end at a critical point. This expectation from symmetry arguments is borne out in the Ginzburg-Landau phase diagram, see right panel of figure(8). This diagram will serve as a basis for our extensions in the following.

2.3 Mass effect without meson condensate

The next systematic step is to include non-zero mass terms as discussed in sections (2.1.2 - 2.1.4) while still "switching off" kaon condensation by setting $\phi = 0$. We can rely on most of the results gained in the previous section, however some interesting and important new results can be worked out. For vanishing kaon condensate, all mass terms except for the linear σ term are simply numerical corrections to the Ginzburg-Landau parameters. We thus absorb these mass terms into new overall prefactors. This reduces the number of independent parameters and does not change the results qualitatively (as before, we do not attempt do determine the complete quantitative effect of the strange quark mass in the full parameter space). Then we can write the potential (104) as:

$$\Omega(\sigma, d) = a_0\sigma + \frac{a}{2}\sigma^2 - \frac{c}{3}\sigma^3 + \frac{b}{4}\sigma^4 + \frac{\alpha}{2}d^2 + \frac{\beta}{4}d^4 - \gamma d^2\sigma \tag{126}$$

Since linear terms have a profound impact on the phase structure, we are no more able to base our analysis on the variation of the coefficients a and α, but also need to consider variations in a_0. These parameters shall be varied without further constraints. The resulting phase diagram would hence in principle be 3 dimensional. In order to illustrate our results in a relatively simple way, we continue to describe our phase diagrams with an (a, α) plane by cutting through the 3 dimensional space at several fixed values of a_0. For notational convenience we have absorbed the factor m_s into the definition of a_0. We then reproduce the known results of figure (7) for the special case $a_0 = 0$. We shall see that several analytical arguments used in the massless case regarding phase transitions and critical points can be used repeatedly also for the more complicated cases. For the complete evaluation of the phase diagram, however, we need to employ numerical calculations.

We now have the following two stationary equations:

$$\frac{\partial\Omega}{\partial d} = a_0 + a\sigma - c\sigma^2 + b\sigma^3 - \gamma d^2 = 0 \tag{127}$$

$$\frac{\partial\Omega}{\partial\sigma} = \alpha d + \beta d^3 - 2\gamma d\sigma = 0 \tag{128}$$

The Hessian remains independent of a_0 and hence is still given by (109).

2.3.1 Nambu Goldstone Phase

The most important difference to the case discussed before lies within the fact, that now in the general case of $a_0 \neq 0$ the NOR phase does no longer exist (we can think of it as the limiting case of $a_0 \to 0$). The quadratic equation determining σ_{min} (116) is now replaced by a cubic one (see equation (127) and set d equal to zero). As in the case of section (2.2), we also find a (semi) analytical curve at the phase boundary to the COE phase, see appendix[2].

We can follow the same procedure as in the last section and introduce a linear shift $\sigma \to \tau = \sigma - \frac{c}{(3b)}$ only this time for the analysis of the NG phase and find:

$$\Omega_{\rm NG}(\tau) = \Omega_0 + a_0^* \tau + \frac{a_c}{2}\tau^2 + \frac{b}{4}\tau^4 \tag{129}$$

with the following abbreviations:

$$\Omega_0 \equiv \frac{a_0 c}{3b} + \frac{ac^2}{18b^2} - \frac{c^4}{108b^3} \tag{130}$$

$$a_0^* \equiv a_0 + \frac{ac}{3b} - \frac{2c^3}{27b^2} \tag{131}$$

$$a_c \equiv a - \frac{c^2}{3b} \tag{132}$$

The cubic equation then simplifies to

$$a_0^* + a_c \tau + b\tau^3 = 0 \tag{133}$$

We now know, that the intersection of the lines determined by $a_0^* = 0$ and $a_c = 0$ represents a critical point at which a first order phase transition line ends. As we can find from equations (132), the resulting crossover between NG and (approximate) NOR phase sets in beyond a critical value for $a_0 = -\frac{c^3}{27b^2}$. In other words, if we plot phase diagrams in the (a, α) plane for fixed values of a_0, this first order line should be absent for all $a_0 < -\frac{c^3}{27b^2}$. In an (a, α) plane, we will rather see a critical vertical line instead of a critical point (which is given in a (a, a_0) plane). This observation is also confirmed by lattice QCD, where it was discovered, that the phase transition to Quark Gluon Plasma (which corresponds to the maximally symmetrical phase, or NOR phase in our terminology) at $\mu = 0$ is indeed a smooth cross-over. Our inclusion of mass terms makes the GL ansatz compatible with these lattice results. We hence also gain a small glimpse on where to place the temperature axis in a speculative translation of our diagram into (T, μ) space (see section 2.3.3). Since also the coexistence phase still ends at critical point (see next section), we can conclude, that the only phase transition line, which does not end at any point is in between the COE and NG phase. The positions of both critical end points are given in figure (10).

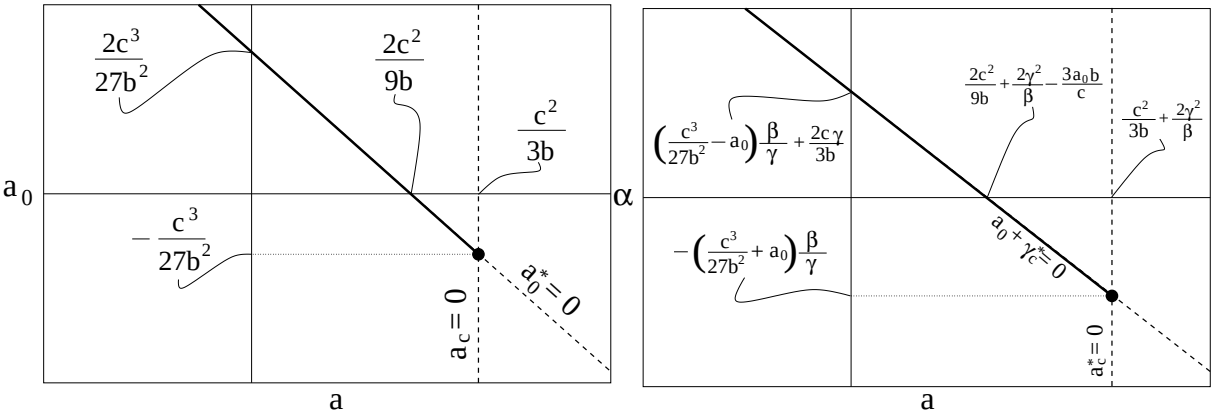

Figure (10): Left panel: first order phase transition line (thick solid line) and critical point in the (a, a_0) plane within the NG phase. The plot shows the coordinates of the critical point and of the intersections of the lines $a_0^* = 0$, $a_c = 0$ with the coordinate axes. Since the NG phase is given by the chiral potential Ω_Φ only, the coordinates depend on the Ginzburg-Landau coefficients b and c, and not on α, β, and γ. In the three-dimensional (a_0, a, α) diagram, the critical point thus becomes a critical line parallel to the α-axis where a first-order phase transition surface ends. Right panel: analogous scenario for the COE phase in the (a, α) plane (note different vertical axes of the two plots!), derived from the potential (129).

2.3.2 Coexistence and CFL Phase

Due to the appearance of the constant term in stationary equation (127) it now is in principle possible to find a "pure" CFL phase ($d \neq 0$ and $\sigma = 0$ at the same time). The diquark condensate then becomes:

$$d^2 = \frac{a_0}{\gamma} \tag{134}$$

Since we require $d^2 > 0$, a CFL phase is possible in case of $a_0 > 0$. Then, the first stationary equation (127) yields a constraint for the parameters:

$$\alpha = -a_0 \frac{\beta}{\gamma} \tag{135}$$

For given a_0, this is simply a straight line in the (a, α) space, where σ vanishes. This line is of no particular interest and we obtain it as a limit case of the COE phase. Both, the NOR and CFL phases exist in a two dimensional subspace of our three dimensional (a, α, a_0) parameter space as they appear as straight lines in an (a, a_0) and (a, α)plane. Anyway this shouldn't be too surprising if we consider, that this results only from the way we choose to plot our phase diagrams. In a (T, μ) diagram, they can still exist within an area of finite extension. In the following discussion we will stick to the three phases we have considered throughout the last sections. We now turn to the coexistence phase.

After inserting $d(\sigma)$ (with $d(\sigma)\,\epsilon\,\mathbb{R}$) into the potential (126) we find:

$$\Omega_{\mathrm{COE}}[\sigma, d^2(\sigma)] = -\frac{\alpha^2}{4\beta} + (a_0 + \gamma^*)\sigma + \frac{a^*}{2}\sigma^2 - \frac{c}{3}\sigma^3 + \frac{b}{4}\sigma^4 \tag{136}$$

where a^* and γ^* are given by (119). In terms of the shifted field τ we have:

$$\Omega_{\mathrm{COE}}(\tau) = \frac{a_0 c}{3b} + \Omega_c + (a_0 + \gamma_c^*)\tau + \frac{a_c^*}{2}\tau^2 + \frac{b}{4}\tau^4 \tag{137}$$

with

$$\Omega_c \equiv -\frac{\alpha^2}{4\beta} + \frac{\gamma^* c}{3b} + \frac{a^* c^2}{18b^2} - \frac{c^4}{108b^3} \tag{138}$$

$$\gamma_c^* \equiv \gamma^* + \frac{a^* c}{3b} - \frac{2c^3}{27b^2} \tag{139}$$

$$a_c^* \equiv a^* - \frac{c^2}{3b} \tag{140}$$

All a_0's are written explicitly. A nonzero a_0 gives additional contributions to the constant and linear terms in τ. All other terms are identical to the massless case (remember that we have absorbed the mass terms in the overall coefficients unless they have produced new structures in the order parameters). The stationary equation is thus

$$a_0 + \gamma_c^* + a_c^*\tau + b\tau^3 = 0 \tag{141}$$

Again we can determine the transition line for the first-order transition within the COE phase and the corresponding critical point. We show the coordinates of this line in the right panel of figure (10) . Besides the disappearance of the critical line between NG and approximate NOR phases (and deformations of the transition lines which do not change the topology of the phase diagram and thus are not very interesting for our purpose) there is one more topological change upon varying a_0: For sufficiently small values of a_0, the first-order line within the COE phase disappears and the phase diagram in the (a, α) plane consists of a sole second-order transition separating NG and COE phases. We can check this by considering the coordinates of the critical point in figure (10): Decreasing a_0 at a fixed anomaly coefficient γ, shifts the critical point towards larger values of α while keeping the a coordinate fixed. We then have to keep in mind, that we only know that the respective phases (NG and COE) are a stationary point of the potential, and we have not yet determined the global minimum. For negative a_0 with sufficiently large modulus, the α coordinate of

the critical point is shifted into a region where the NG phase, not the COE phase, is the ground state, i.e., the critical point has disappeared. Interestingly, at the same value of a_0 where the first order line between NG and approximate NOR phases disappears, the critical point sits on the $\alpha = 0$ axis. We can see this analytically, see also figure(10). Then, upon further decreasing a_0, it approaches the phase transition line between NG and COE phases and disappears for values of a_0 below some critical value for which we do not have an analytic expression. We have thus found two different ways to make the critical point disappear: switching off the anomaly removes the critical point but leaves the first-order critical line, while going to (possibly unphysical) small values of a_0 removes the critical point and the critical line. We illustrate all the topological results of this section in the following series of diagrams for decreasing a_0, which are obtained by numerical evaluation.

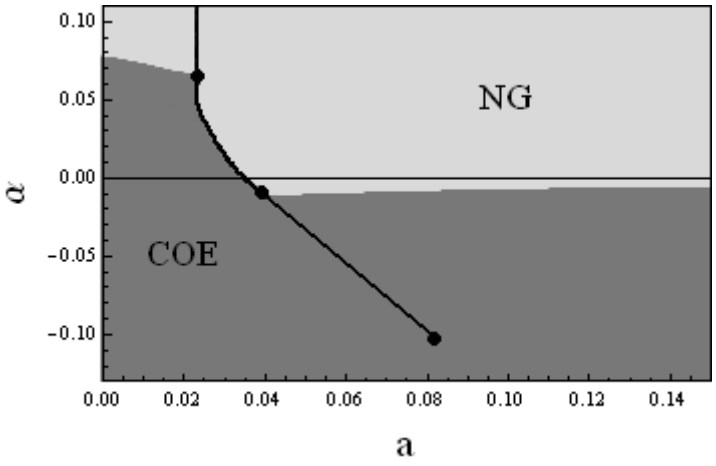

Figure (11): Ginzburg-Landau phase diagrams in the (a, α) plane with quark mass effect in the chiral potential. Black lines are first-order phase transitions. Transitions, which are not marked with a black line are second-order phase transitions. The dots mark the points where a first-order line ends (critical point) and where a second order line terminates at a first-order line (critical endpoint). We choose various values for the linear coefficient a_0 of the chiral condensate, starting with $a_0 = \frac{c^3}{27b^2}$ in the above diagram. All other coefficients remain fixed at the same value as in the right panel of figure(7). In particular, the strength of the couplingγ remains at $\gamma = 0.1$. Intensive numerical studies show, that the qualitative outline of the phase diagram remains unchanged by variations of all other parameters than α and a, which justifies this approach. The parameter a_0 is given in units of $\frac{c^3}{27b^2}$ because for $a_0 < -\frac{c^3}{27b^2}$ the critical line which separates NG and approximate NOR phases vanishes and there is a crossover between these two phases.

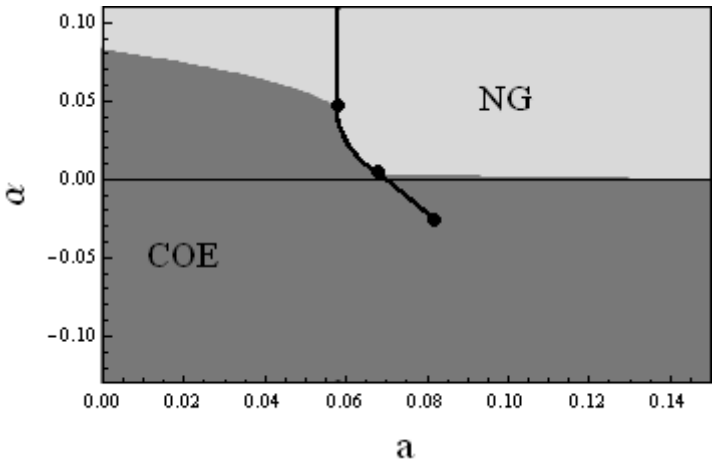

Figure (12): Diagram for $a_0 = -0.5\frac{c^3}{27b^2}$. The critical point approaches the phase-transition line in between COE and NG.

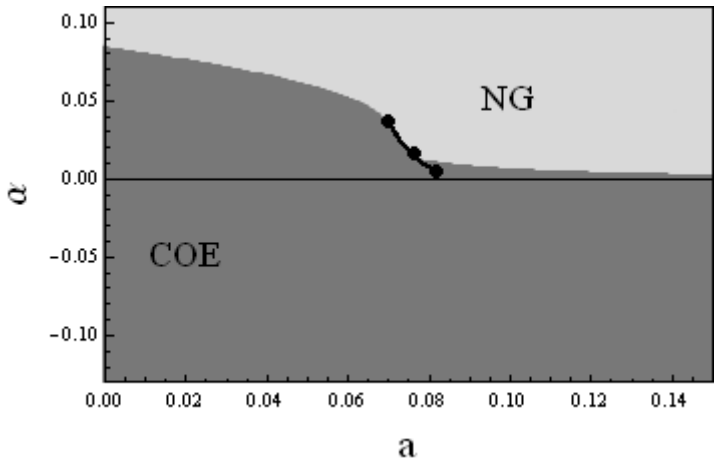

Figure(13): Diagram for $a_0 = -1.1\frac{c^3}{27b^2}$. We have crossed the critical value of $a_0 = -\frac{c^3}{27b^2}$ and the first order phase-transition line separating NG from (approximate) NOR phase has disappeared. The critical point of the COE phase further approaches toward the region occupied by the NG phase.

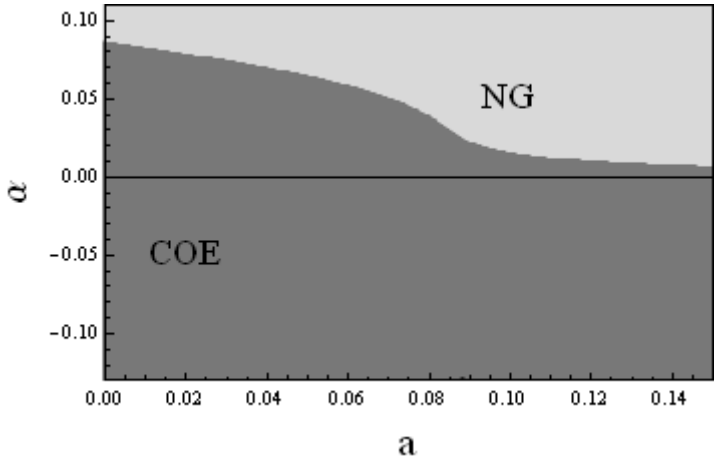

Figure(14): Diagram for $a_0 = -1.8\frac{c^3}{27b^2}$. The critical point has propagated into a region of the phase diagram where the ground state is represented by the NG phase and hence disappeared. At this specific parameter set, there is neither a critical line nor a critical point.

At the end of this chapter, we revisit the analysis of symmetries given in the last section and discuss modifications. First, we notice, that due to the effect of $m_s \neq 0$ the chiral group $SU(3)_L \otimes SU(3)_R$ is now only approximate, which allows for the smooth crossover between COE and (approximate) NOR phase. This is the symmetry based argument for the outline of the diagrams figures (11-14). However, we should mention, that by including only a nonzero strange quark mass $M = (0, 0, m_s)$ instead of the realistic case of $M = diag(m_u, m_d, m_s)$,we would still find different residual groups in NG and COE, since we now have $SU(2)_L \otimes SU(2)_R \otimes U(1)_V$ in COE, where the intact SU(2) symmetry corresponds to the flavors up and down. In the COE phase on the other hand, we use $diag(\sigma, \sigma, \sigma)$ for the chiral condensate, which corresponds to an unbroken vector symmetry $SU(3)_V$. Hence, the crossover should in principle only be visible if we adapt our ansatz for the chiral condensate to $diag(\sigma, \sigma, \sigma_s)$ in order to find the same residual symmetries in both phases. We can check however, that the GL mass terms are equivalent (despite of some irrelevant numerical prefactors) if we choose to set M=diag(m,m,m), in which case we indeed leave the $SU(3)_V$ symmetry intact in both phases.In other words, we reproduce the qualitatively correct result although we are using a simplified ansatz.

2.3.3 Speculative outline of the phase diagram in a (T, μ) plane

The mapping from our (a, α) diagrams into a (T, μ) plane is a dynamical question which, for several reasons, we cannot address within the phenomenological Ginzburg Landau approach. Firstly, the Ginzburg-Landau potential is an expansion in the order parameters and thus cannot account for the complete potential; the expansion is expected to fail far away from second-order phase transitions. Secondly, even if we assume the Ginzburg-Landau approximation to be valid for all temperatures and densities of interest, we would need the dependence of the Ginzburg-Landau coefficients on the baryon chemical potential μ_B and temperature T. This dependence is of course not known within QCD, since the relevant regions of the phase diagram involve strong-coupling effects, and lattice calculations are inapplicable due to the sign problem at finite μ_B. Nevertheless, it is interesting to speculate how the Ginzburg-Landau results translate into the QCD phase diagram. The conjectured translation from the Ginzburg-Landau phase diagrams to QCD is given in figure(15), where the left and middle panel correspond to the situation without strange quark mass, and thus to the Ginzburg-Landau diagrams in figure (8).

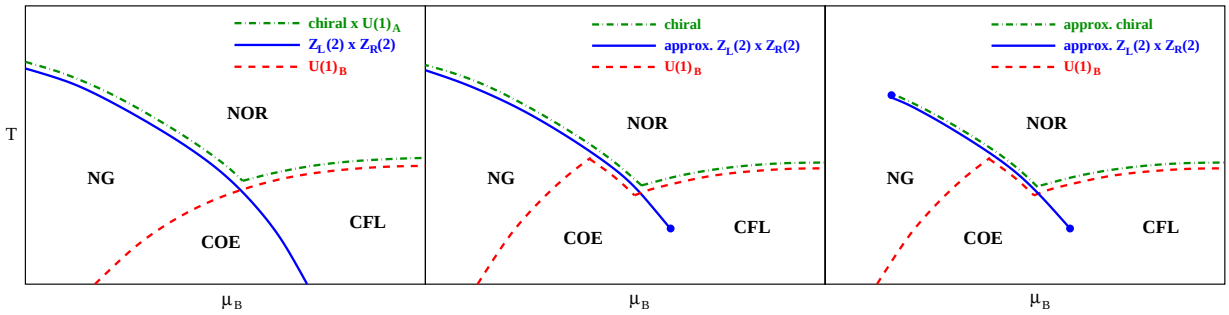

Figure (15): Conjectured translations of the Ginzburg-Landau phase diagrams to the QCD phase diagram in the(μ_B, T) plane [35]. We have indicated the global symmetries which are broken in the various transitions. Left panel: zero quark masses, no instanton effects, corresponding to the left panel in figure (8). Middle panel: zero quark masses, nonzero instanton effects. In this case the CFL and COE phases are no longer distinguished by symmetry and thus allow for a smooth crossover. Whether the critical point is indeed present in the QCD phase diagram cannot be decided from the Ginzburg-Landau study; the $T = 0$ axis may or may not intersect with the first order line in the COE phase in the right panel of figure (8). Here we show the case where it does not. Right panel: nonzero quark masses, nonzero instanton effects, see figures (11-14). Here we know from lattice QCD that the first-order phase transition between NG and (approximate) NOR does not reach the $\mu_B = 0$ axis.

For the interpretation of our Ginzburg-Landau results with strange quark mass, it is helpful to think of the QCD (μ_B, T) plane to be a complicated surface in our (a_0, a, α) parameter space. We know from lattice calculations that, at $\mu_B = 0$, the transition from the chirally broken to the chirally (approximately) symmetric phase is a smooth transition . Therefore, the temperature axis must not intersect the critical surface between NG and (approximate) NOR phases. This critical surface may then manifest itself as a critical line between NG and approximate NOR phases which ends at a critical point, see right panel of figure(15). Another logical possibility is the absence of this line , which would for instance be realized if the whole (μ_B, T) surface were located "behind" the $a_0 = -\frac{c^3}{27b^2}$ plane. For the critical point at low T and large μ_B our analysis with finite strange quark mass has opened up a third possibly topology. Without mass, the point may, although always present in the Ginzburg-Landau phase diagram, be either outside the (μ_B, T) plane (formally, one can think of the point being located at negative T) or within the (μ_B, T) plane. With mass effect we have seen that the critical line that ends at this critical point may be absent in the Ginzburg-Landau phase diagram. Thus, if the (μ_B, T) surface is located at sufficiently negative a_0, there is no first-order transition within the COE phase.

2.4 Phase-diagram including meson condensation

We can now extend the results from the previous sections by allowing for a nonzero kaon condensate ϕ. In principle, this requires to consider several additional independent Ginzburg-Landau parameters as we can see from the full potential (104). In this potential, the parameters α_2, β_2, μ^2, and γ_2 become relevant when we allow for nontrivial values of ϕ. All of these parameters correspond to mass terms and one might, as a first approximation, neglect these terms. However, then the only nontrivial structure involving ϕ is the unsuppressed $d^2\sigma\cos\phi$ term, and there would be no kaon condensation at all (in principle, there could be a condensate at the fixed value of $\phi = \pi$, which, as one can check numerically, never represents ground state). Therefore, we have to keep the $\mu^2\sin^2\phi$ term in order to match our potential to the high-density effective theory, as discussed in section (2.1.3), but for simplicity neglect the terms proportional to α_2, β_2, and γ_2. We have checked numerically that the inclusion of these terms can indeed make a difference to the topology of the phase diagrams with kaon condensate. We shall come back to this issue in the discussion at the end of section(2.5).

Within this approximation, the only additional parameter compared to the previous section is μ^2, and our potential becomes

$$\Omega(\sigma, d, \phi) = a_0\sigma + \frac{a}{2}\sigma^2 - \frac{c}{3}\sigma^3 + \frac{b}{4}\sigma^4 + \frac{\alpha}{2}d^2 + \frac{\beta - \mu^2\sin^2\phi}{4}d^4 - \gamma\frac{1+2\cos\phi}{3}d^2\sigma\,. \tag{142}$$

A comparison with the potential of the high-energy effective theory shows that one can consider the interaction term $d^2\sigma\cos\phi$ as an effective, dynamical mass term for the kaon. The boundedness of the potential requires the d^4 term to be positive, which yields an upper bound for μ^2, $\mu^2 < \beta$. The stationary equations are:

$$\frac{\partial\Omega}{\partial\sigma} = a_0 + a\sigma - c\sigma^2 + b\sigma^3 - \gamma\frac{1+2\cos\phi}{3}d^2 = 0 \tag{143}$$

$$\frac{\partial\Omega}{\partial d} = \alpha d + (\beta - \mu^2\sin^2\phi)d^3 - 2\gamma\frac{1+2\cos\phi}{3}d\sigma = 0 \tag{144}$$

$$\frac{\partial\Omega}{\partial\phi} = d^2\sin\phi\left[\frac{2\gamma}{3}\sigma - \frac{\mu^2}{2}d^2\cos\phi\right] = 0 \tag{145}$$

We distinguish the following phases:

1. NG phase: $\sigma \neq 0$, $d = 0$
2. COE phase: $\sigma \neq 0$, $d \neq 0$, $\phi = 0$
3. COE-K^0 phase: $\sigma \neq 0$, $d \neq 0$, $\phi \neq 0$

The first two phases are the same as in the previous section. Note that ϕ only appears in the potential when d is nonzero. This is clear since without diquark condensation there are no kaons to condense. Therefore, the NG phase does not depend on ϕ. The value of ϕ distinguishes between the phases with nonzero CFL order parameter, COE and COE-K^0. Again, as discussed for the case without meson condensate , the NOR and "pure" CFL/CFL-K^0 phases are obtained as special cases from the NG and COE/COE-K^0 phases and exist in a two-dimensional subspace of the three-dimensional (a_0, a, α) parameter space. The new straight line, on which the CFL phase "lives" in our (a, α) diagrams is given by:

$$\alpha = \frac{-3a_0\left(\beta^2 + 4\mu^4\right)}{4\gamma\left(\beta + \mu^2\right)} \tag{146}$$

In order to compute the phase structure in the presence of a kaon condensate, we need to compute the free energies of the three phases listed above. The results for the NG and COE phases can be taken from the previous section. Thus we only have to discuss the COE-K^0 phase. It is convenient to express ϕ and d as functions of σ. Solving equation (145) for $\cos\phi$ and inserting the result into equation (144) yields

$$\cos\phi(\sigma) = \frac{4\gamma\sigma}{3\mu^2 d^2(\sigma)} \tag{147}$$

$$d^2(\sigma) = \frac{2\gamma\sigma - 3\alpha}{3(\beta - \mu^2)} \tag{148}$$

These expressions can be inserted into equation (143) to obtain an equation for σ. Equivalently, we can insert them into the potential (142) and then minimize it with respect to σ.

The potential becomes

$$\Omega_{\mathrm{COE}-K^0}[\sigma, d(\sigma), \phi(\sigma)] = -\frac{\alpha^2}{4(\beta-\mu^2)} + (a_0+\gamma_\mu^*)\sigma + \frac{a_\mu^*}{2}\sigma^2 - \frac{c}{3}\sigma^3 + \frac{b}{4}\sigma^4\,, \tag{149}$$

where

$$\gamma_\mu^* \equiv \frac{\alpha\gamma}{3(\beta-\mu^2)} \tag{150}$$

$$a_\mu^* \equiv a - \frac{2\gamma^2}{9}\left(\frac{1}{\beta-\mu^2} + \frac{4}{\mu^2}\right) \tag{151}$$

We see that the potential of the COE-K^0 phase has the same structure as the one of the COE phase (137), with modified coefficients γ_μ^*, a_μ^*. We may thus proceed analogously to determine the critical point within the COE-K^0 phase. With the variable $\tau = \sigma - c/(3b)$ from equation (149) we obtain the potential

$$\Omega_{\mathrm{COE}-K^0}(\tau) = \frac{a_0 c}{3b} + \Omega_{c,\mu} + (a_0+\gamma_{c,\mu}^*)\tau + \frac{a_{c,\mu}^*}{2}\tau^2 + \frac{b}{4}\tau^4 \tag{152}$$

with the following coefficients:

$$\Omega_{c,\mu} \equiv -\frac{\alpha^2}{4(\beta-\mu^2)} + \frac{\gamma_\mu^* c}{3b} + \frac{a_\mu^* c^2}{18b^2} - \frac{c^4}{108b^3} \tag{153}$$

$$\gamma_{c,\mu}^* \equiv \gamma_\mu^* + \frac{a_\mu^* c}{3b} - \frac{2c^3}{27b^2} \tag{154}$$

$$a_{c,\mu}^* \equiv a_\mu^* - \frac{c^2}{3b} \tag{155}$$

in complete analogy to equation.The resulting stationary equation after elimination of d and σ is given by:

$$0 = a_0 + \gamma_{c,\mu}^* + a_{c,\mu}^*\tau + b\tau^3\,. \tag{156}$$

Similar to the constraint for d discussed in section (2.2.2) and (2.3.2) we now have to carefully check the angular variable ϕ which means that now, we have to consider two conditions which have to be fulfilled at the same time:

$$d^2(\sigma) > 0 \tag{157}$$

$$-1 < \cos\phi(\sigma) < 1 \tag{158}$$

Since the cubic equation has the same structure as for the COE phase, we obtain an analogous first-order line as shown in section 2.3.2. From $a_0 + \gamma_{c,\mu}^* = a_{c,\mu}^* = 0$ we can compute the location of the critical point. Its (a, α) coordinates turn out to be:

$$a_{\mathrm{COE}-K^0} = \frac{c^2}{3b} + \frac{2\gamma^2}{9}\left(\frac{1}{\beta-\mu^2} + \frac{4}{\mu^2}\right) \tag{159}$$

$$\alpha_{\mathrm{COE}-K^0} = -\frac{3(\beta-\mu^2)}{\gamma}\left(a_0 + \frac{c^3}{27b^2}\right) \tag{160}$$

We can compare this to the critical point in the COE phase whose coordinates are calculated in section (2.3.2):

$$a_{\mathrm{COE}} = \frac{c^2}{3b} + \frac{2\gamma^2}{\beta} \tag{161}$$

$$\alpha_{\mathrm{COE}} = -\frac{\beta}{\gamma}\left(a_0 + \frac{c^3}{27b^2}\right) \tag{162}$$

The phase transition line in between COE and COE-K^0 can again be check by (semi)analytical means, as discussed in appendix [2].

Our next goal is to compute the phase diagram including meson condensation. In particular, the following two questions are of special interest:

1. What is the fate of the critical point in the (a, α) phase diagram in the presence of kaon condensation? We have seen above that a first-order line ending at a critical point is possible in the COE and in the COE-K^0 phase. More precisely, there is a "would-be" critical point with coordinates given in equation (153) which, if the COE phase is the ground state at this point, is a true critical point, and there is a "would-be" critical point with coordinates given in equation (126) which, if the COE-K^0 phase is the ground state at this point, is a true critical point. This leaves us with four logical possibilities. There may be no critical point at all when both "would-be" critical points are covered by the "wrong" phases; there might be one critical point, either in the COE or COE-K^0 phase; or both "would-be" critical points are realized if they are covered by the "right" phases. This classification is very useful since the information about the critical points determines, to a large extent, the topology of the entire phase diagram.
2. Is there a region in the parameter space (here we mean all parameters except for a and α) for which the COE phase is completely replaced by the COE-K^0 phase in the (a, α) plane? This question is interesting in view of the quark-hadron continuity. Recall that the existence of the anomaly-induced critical point opens up the possibility to go, at least at zero temperature, smoothly from the COE phase to the highest-density phase, the (approximate) CFL phase. If we now introduce a meson-condensed phase we might introduce an additional phase transition, separating the COE from the COE-K^0 phase. This phase transition cannot end at a critical point because the kaon condensate breaks strangeness conservation $U(1)_S$ which is an exact symmetry of QCD, i.e., the CFL phases with and without kaon condensation have distinct residual symmetry groups. Only if we take into account the weak interaction which breaks flavor conservation, this line can end at a critical point. Another way of saying this is that through weak interactions the Goldstone mode associated with kaon condensation receives a small mass which has been estimated to be of the order of 50 keV[35]. Here we do not consider such small $U(1)_S$-breaking terms and thus whenever both COE and COE-K^0 phases are present in the phase diagram, they are separated by a true phase transition. Such an additional phase transition could be avoided if the COE phase is completely replaced by the COE-K^0 phase. We shall find that this is never realized in our parameter space.

2.4.1 Critical points with meson condensate

We shall continue to use fixed values for the parameters b,c, and β with respect to which the results are insensitive. To answer question (1) we thus determine for each value of the parameter set (a_0, μ, γ) the number of critical points in the (a, α) plane. To this end, we compute the ground state at the two "would-be" critical points (161/162) and (159/160) and check whether the COE-K^0 phase is the ground state at the point (159/160) and whether the COE phase is the ground state at the point (161/162). This leaves us with 4 possible topologies, which might occur:

- The critical point of the COE phase is located at a position where the COE indeed represents the ground state. We then find one critical point within the COE phase.
- The critical point of the COE-K^0 phase is located at a position where the COE-K^0 indeed represents the ground state. We then find one critical point within the COE-K^0 phase.

- Both critical points are located at positions where the respective phase represents the ground state. We find two critical points, one within the COE and one within COE-K^0 phase.
- No critical point is located at a position where the respective phase represents the ground state. We find no critical point in the phase diagram.

We shall find, that all these cases are realized within our parameter space. As we have learned from previous sections, the existence of the critical point within the COE phase strongly depends on the value of a_0. On the other hand, the space occupied by the COE-K^0 phase (and hence also the probability to observe a critical point in this phase) is naturally linked to the magnitude of the effective kaon chemical potential μ. It is therefore reasonable to distinguish all four cases in a (a_0, μ) plane. We can also check the effect of the coupling by choosing two different values of γ. The results are shown in diagram (16-17).

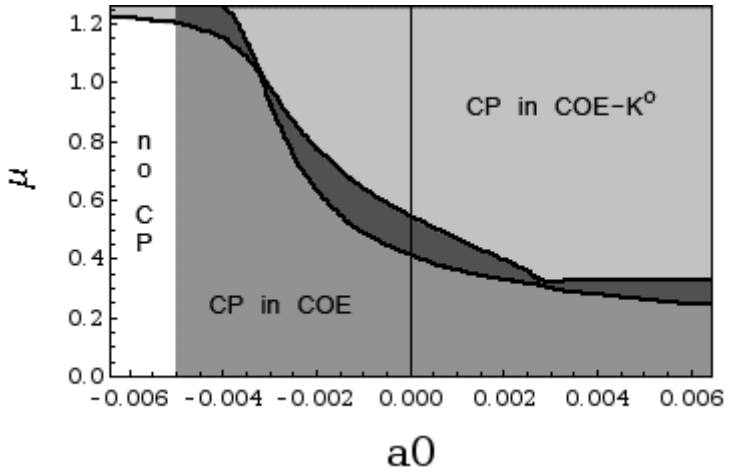

Figure (16): Classification of parameter regions in the (a_0, μ) plane for $\gamma = 0.05$ according to the number of critical points (CP) in the (a, α) plane. Recall that a_0 is the coefficient of the linear term in the chiral condensate, induced by the strange quark mass, μ is the effective kaon chemical potential (bounded from above by $\mu = \beta^{1/2}$ beyond which our Ginzburg-Landau potential becomes unstable), and γ parametrizes the strength of instanton effects. The plot shows four qualitatively different cases each of which is represented by a diagram in figures(18-21). In the dark-gray regions there are, according to our numerical algorithm, two critical points. However, the corresponding phase diagrams show that one of them seems to lie on top of the phase transition line between COE and COE-K^0, see figure(19).

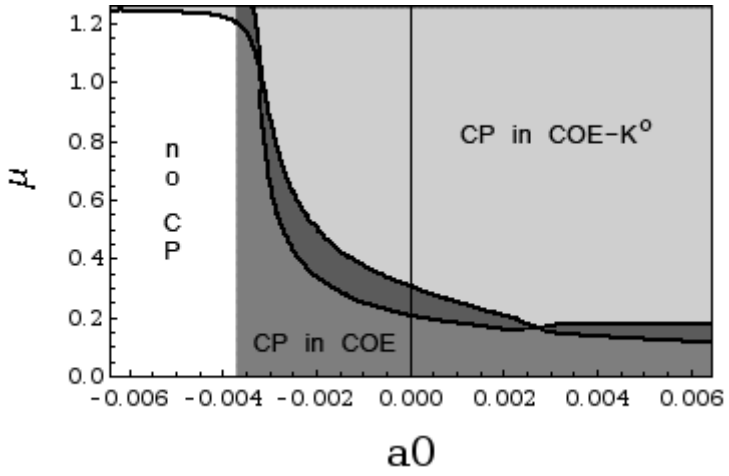

Firgure (17): Classification of parameter regions in the (a_0, μ) plane for $\gamma = 0.1$ according to the number of critical points (CP) in the (a, α) plane. We find, that the region without critical point is shifted toward smaller values of a_0 for increasing γ.

The most obvious observation is that for large μ it is more likely to find the critical point in the kaon condensed phase. The reason is simply that with increasing μ the kaon condensed phase covers more and more space in the phase diagram which supports our interpretation of μ as an effective chemical potential. For sufficiently small values of a_0 there is no critical point at all (except for very large values of μ, just

below its maximum value, for which there is a critical point in the COE-K^0 phase). The reason is the same as already discussed for the COE phase in figure(14): both points (159/160) and (161/162) are in a region where the NG phase is the ground state, and thus they are not realized. Figure(17) shows, that the region without critical points is shifted to smaller values of a_0 for increasing instanton effects, parametrized by γ. We also see that with decreasing instanton effect, it becomes more likely to find the critical point in the meson-condensed phase.

The regions with a critical point in the COE phase are not separated from the regions with a critical point in the COE-K^0 phase by a one-dimensional line. We rather find a two-dimensional region in the (a_0, μ) space where our numerical algorithm finds two critical points, one in each phase. However, a closer look reveals that in this region (dark gray in figures(16/17)) the point (159/160) seems to lie exactly on top of the phase transition line between COE and COE-K^0. In other words, moving within the dark gray areas, the critical point seems to "drag" the second-order phase transition line which is attached to it. Since this is a purely numerical observation, we cannot make a precise statement about the nature of this interesting point. We illustrate this observation below in the context of the corresponding (a, α) phase diagram. Figures (16/17) also show that this two-dimensional region is "squeezed" to a one dimensional point in two instances. The first instance is at $\mu = (\frac{2}{3}\beta)^{1/2}$, $a_0 = -\frac{c^3}{27b^2}$. We can determine this point as follows: Taking into account, that the phase transition line in between COE and COE-K^0 is of second order (which we determine numerically, see in the following section) we consider nonzero, but very small values of ϕ, divide equation (145) by $\sin\phi$ and then set $\cos\phi = 1$ to get a simple relation between σ and d. With the help of equation (148), we eliminate d from this relation and obtain the value of σ at the phase boundary between COE and COE-K^0,

$$\sigma = \frac{3\alpha}{2\gamma}\frac{\mu^2}{3\mu^2 - 2\beta}\,. \tag{163}$$

This relation shows, that for $\mu = (\frac{2}{3}\beta)^{1/2}$ the phase transition line between COE and COE-K^0 is identical with the a axis because in this case σ can only be finite if $\alpha = 0$. Additionally, from equations (159/160) and (160/161) we see that for the parameter values for μ and a_0 from above, the two potential critical points coincide and sit at $\alpha = 0$, i.e., on the a axis. Consequently, both points coincide and lie on the phase separation line. Now, keeping μ fixed and varying a_0 will keep both points together but move them away from the a axis, while the phase transition line remains unchanged. Hence, depending on which direction in a_0 one takes, a critical point will appear either in the COE (smaller a_0) or the COE-K^0 (larger a_0) phase.

The second instance is at positive a_0, and the scenario is quite different here. Now the two critical points do not coincide. Nevertheless, for the given parameters (for $\gamma = 0.1$ we read off $\mu \simeq 0.25\beta^{1/2}$, $a_0 \simeq 0.85\frac{c^3}{27b^2}$) both points lie on the second-order phase transition line between COE and COE-K^0, and again varying the parameters by an arbitrarily small amount creates a critical point in one or the other phase. In contrast to the first instance this is a purely numerical observation.

2.4.2 Phase diagram with meson condensation

We will now illustrate all four qualitatively different scenarios discussed in the previous section in four phase diagrams, corresponding to the cases of one, two or no critical point. The numerical results of all second order phase transition lines (including the new one in between COE and COE-K^0) are in perfect agreement with the results obtain from semi-analytical calculation, discussed in appendix[2]. Not surprisingly, the COE-K^0 phase covers more and more phase space with increasing μ. More interestingly, for all values of μ that are allowed in our approximation, a finite region of the COE phase without meson condensation survives. Here we have increasedμ up to 90% of its upper limit, but we have checked that this conclusion remains valid for all allowed values of μ. This seems to answer the above question 2 of section (2.4) with no, and meson condensation always appears to induce an additional phase transition line which does not end at a critical point. We have checked, however, that this statement depends on our approximation. Taking into account additional terms, for instance the ones proportional to α_2, β_2, γ_2 in equation (104), it is possible to find regions in the parameter space where the COE-K^0 phase completely eliminates the COE phase from the phase diagram. We now systematically investigate for increasing chemical potential μ in figures (18) to (21).

A few remarks need to be made regarding the topology in figure (19). Although our numerical algorithm shows that the COE-K^0 phase is the ground state at the point (159\160), this appears not to be a critical point since there is no first-order line attached to it. Numerically we find that the second-order phase transition between COE and COE-K^0 in the vicinity of this point is very strong, i.e., the kaon condensate

ϕ develops a sizable nonzero value on a much smaller parameter region than it does further away from this point. In other words, the critical point of the COE-K^0 phase behaves like a singular point, at which an otherwise second order phase transition becomes a first order phase transition. This can be seen in figures (22-24) where we compare the order parameters σ, d, and ϕ as a function of a for three fixed values of α. Figure(23) shows the behavior close to the critical point of COE-K^0.

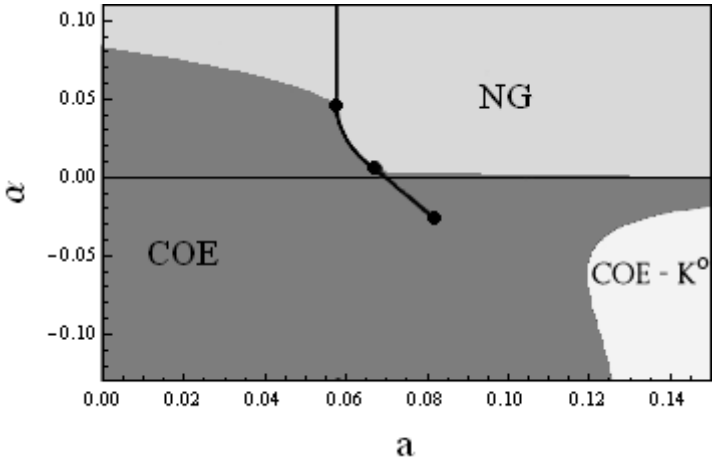

Figure (18): Phase Diagram including strange quark mass and kaon condensation, according to potential (137). a_0 is fixed at a value of $a_0 = -\frac{c^3}{27b^2}$. The maximum value for μ is given by $\mu = \sqrt{\beta}$. We begin with $\mu = 0.35\sqrt{\beta}$. All other parameters remain unchanged in comparison to the previous phase diagrams. In figure (17) we can see, that we expect to find a phase diagram containing one critical point within the COE phase for this set of parameters, which is indeed the case.

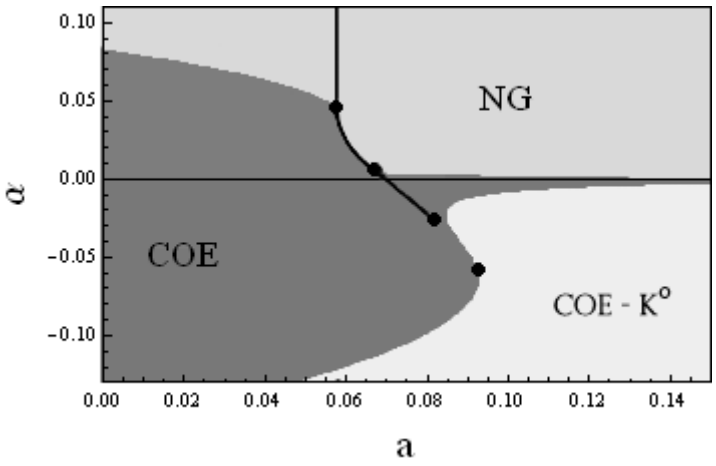

Figure(19): Phase diagram for $a_0 = -\frac{c^3}{27b^2}$ and increased $\mu = 0.5\sqrt{\beta}$. The first trivial observation is, that the expansion of the COE-K^0 phase has increased due to the increase in the effective kaon chemical potential. For this set of parameters, we find ourselves in a region where two critical points coexist in figure (17). It is a numerical observation, that in such a case the critical point of the COE-K^0 phase is always located on top of the phase transition line in between COE and COE-K^0.

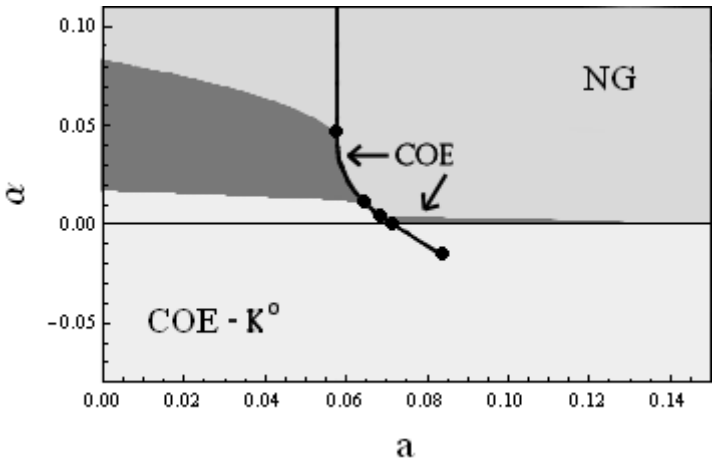

Figure(20). In case of for $a_0 = -\frac{c^3}{27b^2}$ and $\mu = 0.9\sqrt{\beta}$ the COE phase survives in two disconnected regions. From the translation of the (a, α) plane into the QCD phase diagram, as discussed in section (2.3.3), we can expect the $T = 0$ axis to pass through the larger of these two regions, on the left-hand side of the first-order transition. The smaller strip on the right-hand side can be expected to be passed upon heating up the CFL phase, in agreement with NJL model calculations [27]. In both regions it is interesting to check whether a less symmetric color-superconducting phase than CFL becomes favorable. We discuss this possibility in the next section where we include the 2SC phase in our calculation.

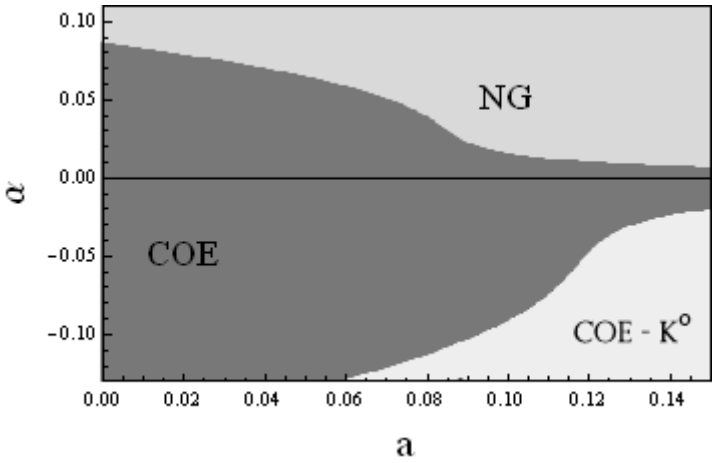

Figure (21): Finally, we set $a_0 = -1.8\frac{c^3}{27b^2}$ and hence behind the critical value at which the phase transition line in between approximate NOR and COE phase ends. This represents the scenario in which there is no critical point.

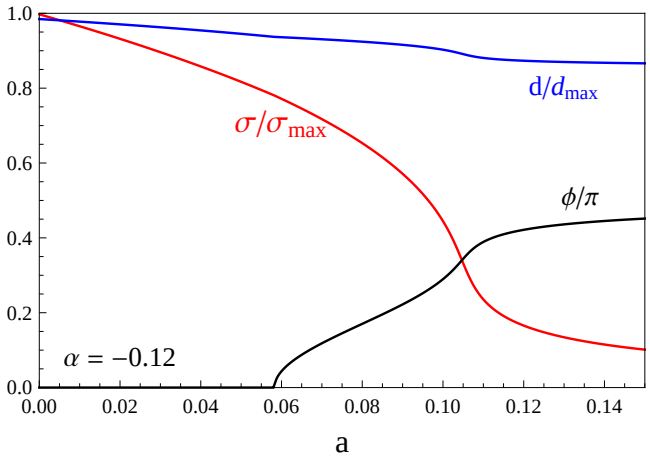

Figure(22): Order parameters plotted for fixed values of $\alpha = -0.12$ (lower than the α coordinate of the critical point). All other parameters are taken from figure(7). As a normalization for the chiral and diquark condensates we have chosen their maximal values in the selected section of the (a, α) phase diagram. These values $\sigma_{\max}$ and $d_{\max}$ are assumed in the lower left corner, i.e., at $(a, \alpha) = (0, -0.13)$. The meson condensate is normalized by its maximum value π.We can also see, that the onset of kaon condensation and crossover (first-order phase transition) to a phase where the approximate $Z_L(2) \times Z_R(2)$ symmetry is restored happen at different values for a.

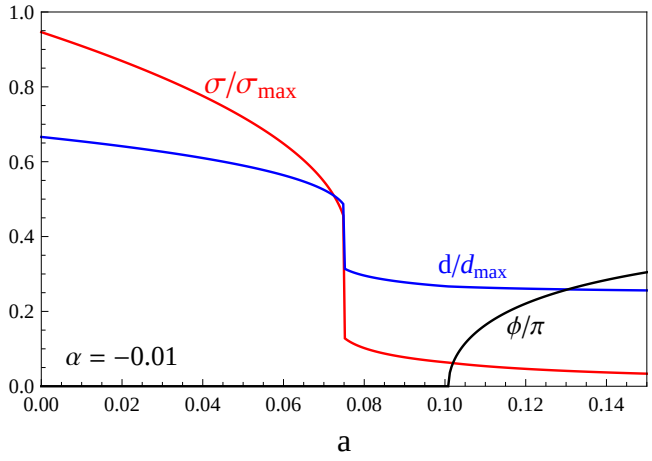

Figure(23): Order parameter plotted for $\alpha = -0.01$ (higher than the α coordinate of the critical point).

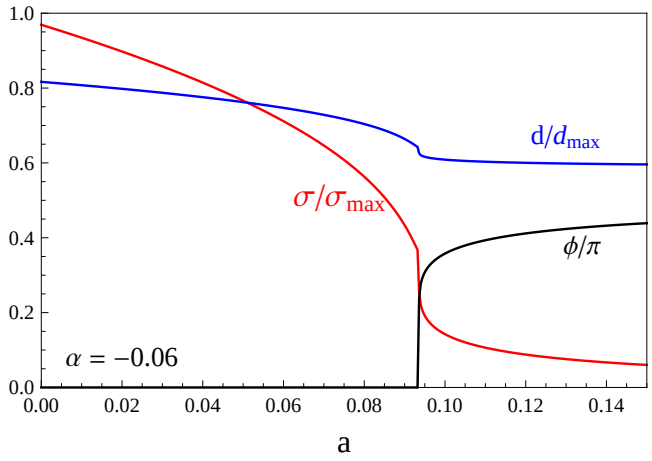

Figure(24): Order parameters plotted for fixed values of $\alpha = -0.06$. This the α position, at which the critical point of the COE-K^0 is located. We can see, that the order parameters (in particular ϕ) do not run smoothly across the a- coordinate of the critical point. We seem to have found a singular point, where the phase transition in between COE and COE-K^0 becomes first order. Here, the onset of kaon condensation and crossover to a phase where the approximate $Z_L(2) \times Z_R(2)$ symmetry is restored happen at the same value for a.

The curves for the order parameters also illustrate the first-order transition at large, but still negative, α (right panel) and its smooth version at small α (left panel). Translated to the QCD phase diagram, we can think of the latter, if present at all, as being closer to zero temperature as the former. In the case of the first-order transition, here taking place in the COE phase, both σ and d are affected significantly. After the transition, the chiral condensate goes to zero for large a. This is as expected because the phase at large a corresponds to the (approximate) CFL-K^0 phase. For the crossover, here taking place in the CFL-K^0 phase, we see that the diquark and meson condensates are not much affected, only the chiral condensate decreases smoothly but drastically. The location of this crossover is given by the continuation of the critical line, see figure(10).

We can rephrase the main conclusion from figures(22-24) in the following concise way. There are basically two transitions: in the first, the chiral condensate goes to approximately zero; this is either a first-order transition or a crossover since the symmetry which gets restored is only approximate in the presence of the axial anomaly. The second is the onset of kaon condensation which is always of second order since the broken symmetry is exact (neglecting weak interactions). The transitions appear at two separate points in figure(22) and (23) (and in different orders, comparing left with right). In figure(24), they appear approximately at the same value of a, which seems to be the reason for the interesting, non-smooth, behavior in this case.

2.5 2SC-Phase

So far our choice of the color-superconducting phases was inspired by high-density arguments. We have considered the CFL phase, which is present at asymptotically large densities, and the kaon condensed CFL phase, which is the first adjustment of the CFL phase to the effect of a small strange quark mass within a weak-coupling approach. Our calculation, however, intends to shed light on the phase structure at moderate densities where less symmetric phases may appear, as discussed in the first chapter. In this section we take into account one of these phases, namely the 2SC phase. In the 2SC phase, all strange quarks as well as all quarks of one color, say blue, remain unpaired, i.e., Cooper pairs are made of red up/green down and green up/red down quarks [36]. At weak coupling and parametrically small strange quark mass the 2SC phase has larger free energy than either CFL or unpaired quark matter [37].Phenomenological models such as the NJL model suggest that this may no longer be true at large coupling [38],[39], and the 2SC phase (or variants thereof) may cover a region in the phase diagram between the low-density chirally broken phase and CFL. The appearance of the 2SC phase would clearly interrupt a possible quark-hadron continuity since 2SC does not break chiral symmetry and thus true phase transitions would be unavoidable between hadronic matter and 2SC and between 2SC and CFL. Building on NJL model calculations with U(1)A-breaking terms [40], [41], it has been argued that the 2SC phase indeed covers the potential anomaly-induced critical point for a wide region in the NJL parameter space [42].

To get an idea about the possibility of a 2SC phase in our general Ginzburg-Landau formalism, we discuss the 2SC phase in the simplest possible way. We shall not attempt to study the whole phase space with 2SC and meson-condensed CFL. This would require the use of several additional Ginzburg-Landau parameters. Without meson condensation we shall be able, however, to make some general statements about the phase diagram including 2SC. On a qualitative level, we give some arguments about the addition of meson condensation at the end of this section.

Without meson condensate, the CFL order parameter is simply $d_L = d_R = \mathrm{diag}(d, d, d)$, which is obtained from the more general order parameter (75) by setting $\phi = 0$. For the 2SC phase, the order parameter is $d_L = d_R = \mathrm{diag}(0, 0, d)$ which describes pairing of only up and down quarks of two colors. In order to compare the free energies of 2SC and CFL we need to go back to the general Ginzburg-Landau terms. We shall for simplicity keep our assumption $\Phi = \mathrm{diag}(\sigma, \sigma, \sigma)$ in both 2SC and CFL. As an alternative ansatz, accounting for the broken flavor symmetry, one might use the ansatz $\Phi = \mathrm{diag}(\sigma, \sigma, 0)$ for the 2SC phase. In this case, the potential becomes trivial because the $d^2\sigma$ term that couples chiral and diquark condensates vanishes, and we have checked numerically that the 2SC phase appears nowhere in the phase diagram. For a more complete study one would have to include the $d^2\sigma^2$ interaction term and/or allow for independent chiral condensates $\Phi = \mathrm{diag}(\sigma_u, \sigma_d, \sigma_s)$. Here we proceed with the symmetric ansatz for Φ and show that the 2SC phase appears in certain regions of the parameter space in accordance with physical expectations and with NJL studies. Our complete ansatz for the 2SC phase is hence given by:

$$d_L = d_R = \mathrm{diag}(0, 0, d) \tag{164}$$
$$\Phi = \mathrm{diag}(\sigma, \sigma, \sigma) \tag{165}$$

Within this ansatz, the chiral part of the potential Ω_Φ can be taken directly from section(2.1.2) and is the same for CFL and 2SC. As for the diquark and interaction part, we find the following potentials:

- Diquark potential:

$$\mathrm{Tr}[d_L d_L^+] = \mathrm{Tr}[d_R d_R^+] = d^2 \tag{166}$$
$$(\mathrm{Tr}[d_L d_L^+])^2 = (\mathrm{Tr}[d_R d_R^+])^2 = \mathrm{Tr}[d_L d_L^+]\mathrm{Tr}[d_R d_R^+] = d^4 \tag{167}$$
$$\mathrm{Tr}[(d_L d_L^+)^2] = \mathrm{Tr}[(d_R d_R^+)^2] = \mathrm{Tr}[d_R d_L^+ d_L d_R^+] = d^4 \tag{168}$$

- Diquark mass-terms:

$$\mathrm{Tr}[d_L^+ M d_R] + h.c. = 2m_s d^2 \tag{169}$$
$$\mathrm{Tr}[d_L^+ M d_R d_R^+ d_R] + h.c. = \mathrm{Tr}[d_L^+ M d_R d_L^+ d_L] + \mathrm{h.c.} = 2m_s d^4 \tag{170}$$
$$\mathrm{Tr}[d_L^+ M d_R]\mathrm{Tr}[d_R^+ d_R] + h.c. = \mathrm{Tr}[d_L^+ M d_R]\mathrm{Tr}[d_L^+ d_L] + \mathrm{h.c.} = 2m_s d^4 \tag{171}$$

- Interaction potential:

$$\mathrm{Tr}[d_R d_L^+ \Phi] + h.c. = 2d^2\sigma \tag{172}$$
$$\mathrm{Tr}[d_L d_L^+ \Phi\Phi^+] = \mathrm{Tr}[d_R d_R^+ \Phi\Phi^+] = d^2\sigma^2 \tag{173}$$
$$\mathrm{Tr}[d_L d_L^+ + d_R d_R^+]\mathrm{Tr}[\Phi^+\Phi] = 6d^2\sigma^2 \tag{174}$$
$$Det\Phi \mathrm{Tr}[d_L d_R^+ \Phi^{-1}] + h.c. = 2d^2\sigma^2 \tag{175}$$

- Interaction mass-terms:

$$\mathrm{Tr}[d_L d_L^+ M\Phi] + h.c. = 2d^2\sigma m_s \tag{176}$$
$$\mathrm{Tr}[d_L d_L^+ + d_R d_R^+]Tr[M^+\Phi] + h.c. = 4d^2\sigma(m_u + m_d + m_s) \tag{177}$$
$$\epsilon_{abc}\epsilon_{ijk} M_{ai}\Phi_{bj}(d_L d_R^+)_{ck} = d^2\sigma(m_d + m_u) \tag{178}$$

In the construction of the full diquark potential potential,

$$\begin{aligned}\Omega_d = {} & \alpha_1\left(\mathrm{Tr}[d_L d_L^+] + \mathrm{Tr}[d_R d_R^+]\right) + \alpha_2\left(\mathrm{Tr}[d_L^+ M d_R] + \mathrm{h.c.}\right) \\ & + \beta_1\left\{(\mathrm{Tr}[d_L d_L^+])^2 + (\mathrm{Tr}[d_R d_R^+])^2\right\} + \beta_2\mathrm{Tr}[d_L d_L^+]\mathrm{Tr}[d_R d_R^+] + \beta_3\left\{\mathrm{Tr}[(d_L d_L^+)^2] + \mathrm{Tr}[(d_R d_R^+)^2]\right\} \\ & + \beta_4\mathrm{Tr}[d_R d_L^+ d_L d_R^+] + \beta_5\left(\mathrm{Tr}[d_L^+ M d_R d_R^+ d_R] + \mathrm{h.c.}\right) + \beta_6\left(\mathrm{Tr}[d_R^+ M d_L d_L^+ d_L] + \mathrm{h.c.}\right) \\ & \beta_7\left(\mathrm{Tr}[d_L^+ M d_R]\mathrm{Tr}[d_R^+ d_R] + \mathrm{h.c.}\right) + \beta_8\left(\mathrm{Tr}[d_L^+ M d_R]\mathrm{Tr}[d_L^+ d_L] + \mathrm{h.c.}\right)\end{aligned} \tag{179}$$

We have assumed the coefficients in front of terms that are related by an exchange of L and R to be identical. Here, α_1 and α_2 are the coefficients for the d^2 terms without and with mass insertion, and $\beta_1, \ldots, \beta_4$ and $\beta_5, \ldots, \beta_8$ are the coefficients for the d^4 terms without and with mass insertions. For the interaction terms (we neglect again the $d^2\sigma^2$ terms) we obtain:

$$\begin{aligned}\Omega_{\Phi d} = {} & \gamma_1\left(\mathrm{Tr}[d_R d_L^+ \Phi] + \mathrm{h.c.}\right) + \gamma_2\left(\mathrm{Tr}[d_L d_L^+ + d_R d_R^+]\mathrm{Tr}[M^+\Phi] + \mathrm{h.c.}\right) \\ & + \gamma_3\left(\mathrm{Tr}[d_L d_L^+ M\Phi] + \mathrm{h.c.}\right) + \gamma_4\left[\epsilon_{abc}\epsilon_{ijk} M_{ai}\Phi_{bj}(d_L d_R^+)_{ck} + \mathrm{h.c.}\right]\end{aligned} \tag{180}$$

with γ_1 and $\gamma_2, \ldots, \gamma_4$ being the coefficients for the terms without and with mass insertions. We use the explicit computation of the traces shown above and write the 2SC and CFL potentials as

$$\Omega_{\mathrm{CFL}} = \Omega_\Phi + (\alpha_1 + \alpha_2 m_s)d^2 + (\beta_1^{\mathrm{CFL}} + \beta_2^{\mathrm{CFL}} m_s)d^4 + (\gamma_1 + \gamma_2^{\mathrm{CFL}} m_s)d^2\sigma \tag{181}$$
$$\Omega_{\mathrm{2SC}} = \Omega_\Phi + \left(\tfrac{\alpha_1}{3} + \alpha_2 m_s\right)d^2 + (\beta_1^{\mathrm{2SC}} + \beta_2^{\mathrm{2SC}} m_s)d^4 + \left(\tfrac{\gamma_1}{3} + \gamma_2^{\mathrm{2SC}} m_s\right)d^2\sigma \tag{182}$$

where we have used the fact, that (apart from $a_0^{CFL} = a_0^{2SC},\ a_{CFL} = a_{2SC},\ b_{CFL} = b_{2SC},\ c_{CFL} = c_{2SC}$) there are simple relations between the coefficients α_1 , $\alpha_2$and γ_1 in both phases:

$$\alpha_1^{CFL} = \tfrac{1}{3}\alpha_1^{2SC} \tag{183}$$
$$\alpha_2^{CFL} = \alpha_2^{2SC} \tag{184}$$
$$\gamma_1^{CFL} = \tfrac{1}{3}\gamma_1^{2SC} \tag{185}$$

However, the coefficients $\beta_1^{\mathrm{CFL/2SC}}$, $\beta_2^{\mathrm{CFL,2SC}}$ and $\gamma_2^{CFL/2SC}$ consist of many different contributions as we can see from equations (179) and (180).

The overall ratio between the α and γ coefficients and their mass corrections in both phases can be written by an expansion in m_s:

$$\frac{\alpha_1^{CFL}+\alpha_2^{CFL}m_s}{\alpha_1^{2SC}+\alpha_2^{2SC}m_s}=\frac{\alpha_1+\alpha_2 m_s}{\frac{1}{3}\alpha_1+\alpha_2 m_s}=\frac{1+\frac{\alpha_2}{\alpha_1}m_s}{\frac{1}{3}+\frac{\alpha_2}{\alpha_1}m_s}=3-6\frac{\alpha_2}{\alpha_1}m_s+18(\frac{\alpha_2}{\alpha_1})^2m_S^2+O((m_s)^3) \quad (186)$$

$$\frac{\gamma_1+\gamma_2^{CFL}m_s}{\bar{\gamma}_1+\gamma_2^{2SC}m_s}=\frac{1+\frac{\gamma_2^{CFL}}{\gamma_1}m_s}{\frac{1}{3}+\frac{\gamma_2^{2SC}}{\gamma_1}m_s}=3+3(\frac{\gamma_2^{CFL}}{\gamma_1}-3\frac{\gamma_2^{2SC}}{\gamma_1})m_s+O(m_s^2) \quad (187)$$

where $\gamma_2^{CFL}=2(\gamma_2+6\gamma_3+\gamma_4)$ and $\gamma_2^{2SC}=2(\gamma_2+2\gamma_3)$ in terms of equation (150). For our numerical purpose, it is of course irrelevant how the composite coefficients depend on the original ones. The important point is, that including a small mass term corresponds to a small correction to this fixed ratio of $1/3$ for α_1 and γ_1 as shown by the expansion above. Such a statement is not possible for the d^4 terms where in general we need independent parameters even for the mass-independent terms. Hence, the overall coefficient in front of the d^4 term in the 2SC phase must be taken as a new parameter and cannot be expressed in terms of a single coefficient of the CFL phase. Fortunately, we can check, that our results are (qualitatively) insensitive to variations of coefficients $\propto d^4$ on a large scale whereas variations of terms $\propto d^2$ and $\propto d^2\sigma$ lead to significant changes as we will discuss below. We shall therefore use the following convenient way to include the 2SC phase into our phase diagram:

$$\Omega_{2\mathrm{SC}}(\sigma,d)=a_0\sigma+\frac{a}{2}\sigma^2-\frac{c}{3}\sigma^3+\frac{b}{4}\sigma^4+\frac{\alpha}{2}\left(\frac{1}{3}+\tilde{\alpha}m_s\right)d^2+\frac{\beta}{4}d^4-\gamma\left(\frac{1}{3}+\tilde{\gamma}m_s\right)d^2\sigma \quad (188)$$

We have explicitly included effects of mass corrections to α and γ and ignored corrections to β. We can now proceed analogously to the previous sections and determine the ground state of the system. Now we need to compare the NG, COE(CFL), and COE(2SC) phases, where COE(CFL) is the phase with coexisting chiral condensate σ and diquark condensate in the CFL pattern (this phase was simply termed COE in the previous sections), and COE(2SC) is the phase where σ coexists with the diquark condensate in the 2SC pattern. The main question is under which conditions and where in the phase diagram the 2SC phase appears. We summarize the results of our numerical studies and illustrate them in figures (25) and (26).

- If we neglect the mass corrections to the d^2 and $d^2\sigma$ terms, i.e.,$\tilde{\alpha}=\tilde{\gamma}=0$ in equation (188), there is no 2SC phase in our (a,α) phase diagram for all values of a_0. In other words, the mass effect through the linear term in the chiral potential $\propto a_0$ is not sufficient to trigger the 2SC phase. More mass corrections are needed.
- As soon as mass corrections $\tilde{\alpha}<0$ or $\tilde{\gamma}>0$ or both are switched on, there is at least one region in the (a,α) phase diagram for all a_0 where the 2SC phase is the ground state. (It is a numerical observation that only the given signs of $\tilde{\alpha}$, $\tilde{\gamma}$ yield the results shown in figure(25) and (26); different signs, i.e., $\tilde{\alpha}>0$ and/or $\tilde{\gamma}<0$ require sufficiently large positive values of a_0 for the 2SC phase to appear.) The 2SC phase appears in the expected regions of the phase diagram, separating the NG phase from the CFL phase. This is shown in figures (25\26) for two different values of $a_0<0$. Increasing $|a_0|$ for negative a_0 increases the area which is covered by the 2SC phase.
- The phase transition from COE(CFL) to COE(2SC) is of first order. This is clear since two of the gap parameters must change discontinuously in the transition from $d_L=d_R=\mathrm{diag}(d,d,d)$ to $d_L=d_R=\mathrm{diag}(0,0,d)$. Additionally, our numerical results show that the chiral condensate is discontinuous at this transition.

It is an interesting question whether meson condensation can prevent the 2SC phase from appearing. Comparing figures(18-21) and figures(25,26), the answer seems to be no because the COE-K^0 phase does not reach areas close to the transition to the NG phase, and this is exactly where the 2SC phase lives. However, we have to remember that in our discussion of kaon condensation we have neglected all mass terms except for a_0 and the one associated with the kaon chemical potential. The omitted terms are exactly the ones that are needed to obtain the 2SC phase. Hence we would have to redo our analysis, including 2SC and kaon condensation and taking into account the mass corrections for the d^2 and $d^2\sigma$ terms in the potential (104). This would introduce more independent parameters and without further constraints a systematic study would be very unwieldy. Therefore, we have only done some numerical calculations with selected parameters. These calculations show that if we take for instance one of the phase diagrams in figures (25/26)

, there is a range of parameters for the mass corrections where the kaon-condensed phase does expel the 2SC phase. However, the 2SC phase is only expelled completely from the(a, α) phase diagram if the mass corrections $\propto \alpha_2, \beta_2, \gamma_1, \gamma_2$ in equation are of the order of or larger than the $\mathcal{O}(m_s^0)$ terms. In this case, our Ginzburg-Landau expansion becomes unreliable since we have neglected mass terms of higher order (except for the term $\propto \mu^2$ which is suggested to be relevant from high-density arguments, as explained). If we keep the mass corrections much smaller than the $\mathcal{O}(m_s^0)$ terms, the 2SC phase, if it is preferred over the CFL phase in some region of the phase diagram, also appears to be favored (in a smaller region) over the CFL-K^0 phase.

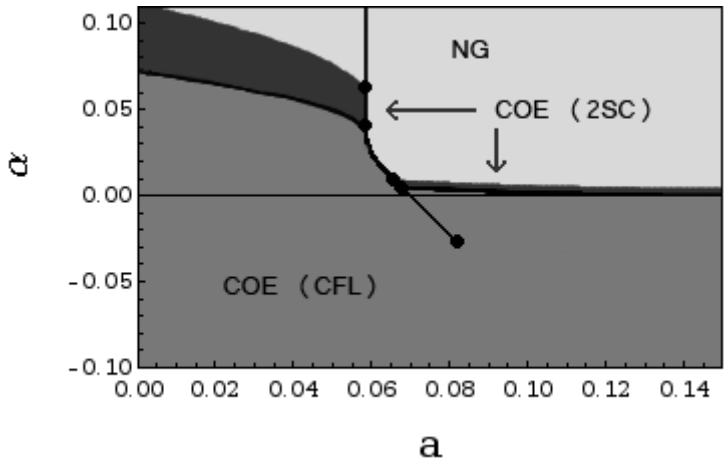

Figure(25): Phase diagram including 2SC for $a_0 = -0.5\frac{c^3}{27b^2}$. Again, we set up all other parameters the same way as in the previous diagrams. The 2SC phase occurs after including mass corrections according to the potential (188), for these plots we have chosen $-\tilde{\alpha}m_s = \tilde{\gamma}m_s = 0.05$. As a function of increasing $|a_0|$ ($a_0 < 0$) the 2SC phase first appears on the left-hand side of the phase transition between NG and COE, then additionally in a disconnected region on the right-hand side , before the two regions merge for sufficiently large $|a_0|$ (see below). COE(CFL) denotes the phase with nonzero chiral condensate and diquark condensate in the CFL phase (denoted simply COE in all previous plots), COE(2SC) denotes the phase with nonzero chiral condensate and diquark condensate in the 2SC phase. The transition in between COE(2SC) an COE (CFL) is of first order (us usually indicated by an enforced black line). Had we not taken into account the 2SC phase, the (second-order) transition between COE and NG would have been between the shown COE(CFL)/COE(2SC) and COE(2SC)/NG transitions. In this sense, the 2SC phase extends the color-superconducting area.

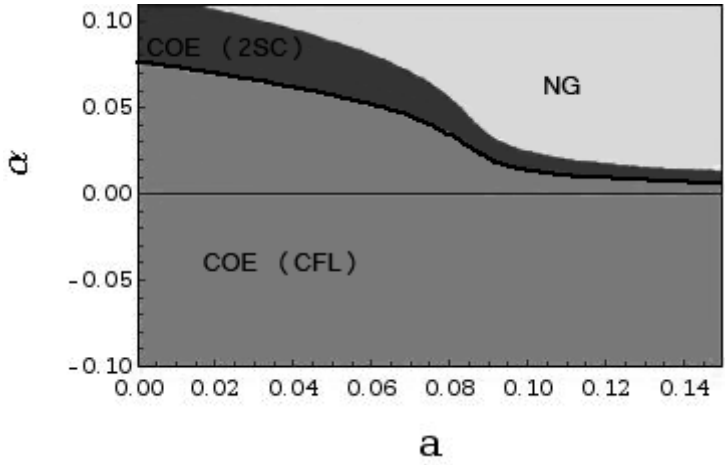

Figure(26): Phase diagram including 2SC for $a_0 = -1.8\frac{c^3}{27b^2}$. This scenario corresponds to the case discussed in diagrams (14) and (11). The two separated region of 2SC have merged.

Chapter 3

Summary and Outlook

We have studied phases of dense matter in a Ginzburg-Landau approach. Previous Ginzburg-Landau studies have shown that the axial anomaly may induce a high-density critical point in the QCD phase diagram, possibly leading to a smooth crossover between hadronic matter and color-flavor locked quark matter. We have explained in detail that the existence of this critical point is a consequence of the (discrete) symmetry of the CFL phase which – in the presence of the axial anomaly – is not changed by adding a chiral condensate. Our main goal has been to extend the previous studies by including a strange quark mass. We have discussed several different, although related, mass effects.

Firstly, the strange quark mass introduces a term linear in the chiral condensate σ, say $a_0\sigma$, which allows for a smooth crossover between the phases of broken and (approximately) restored chiral symmetry. This effect is most relevant for the high-temperature, low-density phase of QCD where there is indeed such a crossover between the hadronic phase and the Quark-Gluon Plasma, as we know from lattice calculations. We have shown that the term $a_0\sigma$ is also relevant for the high-density critical point. The reason is the anomalous interaction term that couples the chiral to the diquark condensate d, say $\gamma d^2\sigma$. For sufficiently large values of $|a_0|$ ($a_0 < 0$) the first-order phase transition line which, for nonzero γ, ends at the high-density critical point disappears. As a result the transition between the ordinary chirally broken phase and the CFL phase is smooth everywhere.

Secondly, a nonzero strange quark mass is expected to induce less symmetric color-superconducting phases. In high-density calculations, the CFL-K^0 phase is the first phase that appears after going down in density from the asymptotically dense CFL region. We have introduced a kaon condensate as a relative rotation of left- and right-handed diquark condensates and have adjusted the Ginzburg-Landau potential to match the essential terms of the high-density effective theory. We have identified the region in the parameter space where the critical point has moved from the CFL into the CFL-K^0 phase and have determined the location of both possible critical points in the presence of a strange quark mass. In addition to a shift of the critical point, the kaon condensate introduces a true phase transition because it breaks strangeness conservation spontaneously which is an exact symmetry in QCD. For future studies it would be interesting to also consider terms in the Ginzburg-Landau potential which explicitly break strangeness, to account for (small) effects of the weak interaction.

Thirdly, we have discussed a more radical reaction of the system to a nonzero strange quark mass, namely the appearance of the 2SC phase. In previous studies in the Ginzburg-Landau approach, it has been shown that for infinitely large strange quark mass there cannot be a high-density critical point. The reason is that the 2SC phase does not break chiral symmetry and thus there must be a true phase transition between the 2SC phase with and without coexisting chiral condensate. Since we have included a nonzero, but finite, strange quark mass, we could study the competition between the 2SC and CFL phases under the influence of a nonzero chiral condensate. We have shown that the mass term$a_0\sigma$ is not sufficient to favor the 2SC phase in any part of the phase diagram. Additional mass terms, which we have neglected in our discussion of the meson condensate, are necessary for the 2SC phase to appear between unpaired quark matter and the CFL phase. In a conjectured translation to the QCD phase diagram it seems that the 2SC phase appears "first" (i.e., for the smallest values of these mass terms) at low temperature. As a consequence, the smooth crossover at zero temperature between hadronic and quark matter would be disrupted by true phase transitions. The appearance of the 2SC phase is in agreement with recent NJL model calculations.

There are several possible extensions of our work. We have studied the competition between 2SC and CFL systematically, but have only briefly discussed the competition between 2SC and CFL-K^0. For a more complete analysis it would be helpful to first find some constraints for the additional Ginzburg-Landau parameters. The potential proliferation of parameters has also led us to a simplified, flavor-symmetric ansatz for the chiral condensate. One should check in further studies how our results change with a more realistic ansatz. It would also be interesting to consider different meson condensates and possibly their coexistence. This is important since we do not know the masses of the CFL mesons at intermediate densities, and it may well be a different meson than the kaon which condenses in this regime. Furthermore, one should also take into account the requirement of electric and color neutrality. This was not an issue in our calculations with the CFL phase since this phase is automatically neutral (and a neutral kaon condensate does not change this).

In the 2SC phase, however, the numbers of up, down, and strange quarks are not identical, and the existence and details of this phase (as for any non-CFL color superconductor) depend strongly on the neutrality constraint. In our general Ginzburg-Landau approach the definition of charge is not straightforward since one would need the dependence of the Ginzburg-Landau parameters on the various chemical potentials, either from weak-coupling calculations or from a phenomenological model.

More generally speaking, the Ginzburg-Landau approach, including possible extensions in the future, is an interesting model-independent alternative to NJL model studies regarding the QCD phase diagram at low temperature and large, but not asymptotically large, densities. Both approaches, however, are far from being conclusive for the actual, full QCD situation. Therefore, it is important to also pursue other approaches such as improvements of perturbative calculations [43] or studies of dense matter in the astrophysical context and comparing properties of phases of dense (quark) matter with data from compact stars [44],[45].

Appendix 1

High density effective Meson masses

In order to determine the mass ordering of the effective meson masses, we follow the steps of reference [13/14]. We need to evaluate the following mass term of the high density effective Lagrangian, discussed in section (1.5.5):

$$\Delta\mathcal{L}_{eff} = \frac{af_\pi^2}{2} detMTr[M^{-1}\Sigma] + h.c. \tag{189}$$

We start by expanding the chiral field Σ:

$$\Sigma = e^{i\theta_a\lambda_a/f_\pi} = 1 + i\frac{\theta_a\lambda_a}{f_\pi} - \frac{\theta_a\theta_b\lambda_a\lambda_b}{2f_\pi^2} + ... \tag{190}$$

where we are interested in terms quadratic in the fields θ_i. As usual, the λ_i are Gellmann matrices. Additionally, we include $\lambda_9 = \sqrt{\frac{2}{3}}$ in order to take into account the singlet state of $\eta^{`}$. We can then read off the mass matrix :

$$\frac{1}{2}M_{ab}^2\theta^a\theta^b = \frac{C}{2} detMTr[M^{-1}\lambda_a\lambda_b]\theta_a\theta_b \tag{191}$$

where $C \sim 1.578$ has been calculated in reference [13]. The explicit evaluation of the 9×9 matrix yields a block diagonal structure of three 2×2 blocks and one 3×3 matrix. The 2×2 blocks corresponding to the fields (θ_1,θ_2), (θ_4,θ_5), (θ_6,θ_7) are given for a high density effective mass term (left) and compared to the chiral effective mass term in (34) (right):

$$\begin{pmatrix} m_s(m_u+m_d) & im_s(m_d-m_u) \\ im_s(m_u-m_d) & m_s(m_u+m_d) \end{pmatrix} \quad \begin{pmatrix} (m_u+m_d) & i(m_u-m_d) \\ i(m_d-m_u) & (m_u+m_d) \end{pmatrix} \tag{192}$$

$$\begin{pmatrix} m_u(m_s+m_d) & im_u(m_s-m_d) \\ im_u(m_d-m_s) & m_u(m_s+m_d) \end{pmatrix} \quad \begin{pmatrix} (m_u+m_s) & i(m_u-m_s) \\ i(m_s-m_u) & (m_u+m_s) \end{pmatrix} \tag{193}$$

$$\begin{pmatrix} m_d(m_s+m_d) & im_d(m_s-m_u) \\ im_d(m_u-m_s) & m_d(m_s+m_d) \end{pmatrix} \quad \begin{pmatrix} (m_s+m_d) & i(m_d-m_s) \\ i(m_s-m_d) & (m_d+m_s) \end{pmatrix} \tag{194}$$

and the 3×3 block corresponding to $(\theta_3,\theta_8,\theta_9)$ is given by:

$$\begin{pmatrix} m_s(m_u+m_d) & \frac{1}{\sqrt{3}}m_s(m_d-m_u) & \sqrt{\frac{2}{3}}m_s(m_d-m_u) \\ \frac{1}{\sqrt{3}}m_s(m_d-m_u) & \frac{1}{3}(m_dm_s+m_um_s+4m_dm_u) & \frac{\sqrt{2}}{3}(m_dm_s+m_um_s-2m_dm_u) \\ \sqrt{\frac{2}{3}}m_s(m_d-m_u) & \frac{\sqrt{2}}{3}(m_dm_s+m_um_s-2m_dm_u) & \frac{2}{3}(m_dm_s+m_um_s+m_dm_u) \end{pmatrix} \tag{195}$$

We analyze the structure of the the 2×2 blocks which is very simple as we can see from (192 - 194):

$$\begin{pmatrix} A & iB \\ -iB & A \end{pmatrix} \tag{196}$$

with eigenvalues $\lambda_{1,2} = A \pm B$ and eigenvectors $\theta_1 \pm i\theta_2$, $\theta_4 \pm i\theta_5$, $\theta_5 \pm i\theta_6$ corresponding to the eigenstates of $\pi^\pm$, $K^\pm$ and $K^0/\bar{K}^0$. Considering, that these eigenvalues correspond to the meson masses squared, a pion mass term for example would then have to be constructed as follows:

$$m_{\pi^\pm}^2\theta_{\pi^\pm}^2 = \propto (A+B)\left\|(\theta_1 - i\theta_2)\right\|^2 + (A-B)\left\|(\theta_1+i\theta_2)\right\|^2 = 2A\theta_{\pi^\pm}^2$$

where we have used the fact, that any member of the group U(3) is represented by $e^{i\lambda_a\theta_a}$ with $\theta_a \in \mathbb{R}$. The mass terms of $\pi^{\pm}$ are hence proportional to A, where A is taken from matrix (192\left) $A = m_s(m_u + m_d)$. Similar considerations apply for the particle content of all 2×2 blocks which confirms the mass ordering introduced in chapter (1.5.4). For the 3×3 block corresponds to the particle content of η, $\eta^{`}$ *and* $\pi^0$. For these cases one has to perform a numerical diagonalization. Additionally, one also has to take into account the effect of the axial anomly, which leads to the unusual heavy $\eta^{`}$ mass.

Appendix 2

Numerics

Through out this entire work we often rely on numerical calculations of phase diagrams since we either don't posses any analytical expression for phase transitions line or the corresponding expressions are simply to complicated to be analyzed analytically. The first case is illustrated by the curve labeled "numerics" in figure (7). This is indeed the only region for which we cannot find any analytical solution-not even in principle. The second situation often occurs because in the general case we are forced to deal with solutions to cubic equations after minimizing the full potential . We will now briefly discuss the basic idea of the numerical algorithm and provide semi-analytical methods to check our numerical results. In order to construct a phase diagram, we execute the following steps:

- Since we scan all phases within an (a, α) plane for fixed values of a_0, we need to set up a discrete lattice for a and α and loop over all values within this lattice. All other constants remain at a fixed value.
- We use an expression, in which we have already minimized our potential in ϕ and d, $\Omega(\sigma, \phi(\sigma), d_{min}(\sigma))$, minimize this potential in σ and solve the stationary equation and evaluate $\Omega(\sigma_{min})$ repeatedly for all values of a and α. Since this is a cubic equation in σ, we have to consider three potential solutions. Either one or all three of them are real.
- We pick out only the real solutions we get from the second step and check, if the following constraints are fulfilled: $d^2(\sigma_{min}) > 0, \quad -1 < \cos\phi(\sigma) < 1$. Solutions which violate one or both conditions are rejected. The conditions of $d^2(\sigma_{min}) > 0$ is of course different for COE(2SC), COE(CFL) and COE-K^0.
- We now calculate all the energy of the ground state of all phases and all possible solutions, compare them, and pick the one with the lowest value.
- We ask, which phase represents the overall ground state for a fixed value of a and α and then assign numbers to the specific phases (for example if the ground is represented by the NG phase, assign "1" to the phase parameter). All positions (a, α), at which this number changes, are saved in an array.

additionally, we can specifically ask for first order transitions. In this case we have to monitor all order parameters (especially σ). If $|\sigma|$ has increased by, lets say, ten times compared to the last (a, α) position, we mark this point as first order. In addition to these purely numerical results, we have developed some semi-analytical approaches to confirm our findings.

- We can make use of Hessian an determine the phase transition line as discussed in section 2.2.1. Even in the more complicated case, where σ_{min} in $\alpha = 2\gamma\sigma(a)_{min}$ is given by a cubic equation, we can, at least numerically, plot the analytical curve $\alpha(a)$ in order to determine the phase transition-line in between COE(CFL) and NG as well as COE(2SC). The result is illustrated in figure A1 and A2.
- A semi-analytical expression for the phase transition line between the COE and COE-K^0 phases can be found if we follow the steps in section 2.4.1 leading to equation 163. There we have determined the value of σat the phase boundary between COE and COE-K^0 to be

$$\sigma = \frac{3\alpha}{2\gamma}\frac{\mu^2}{3\mu^2 - 2\beta}.$$

  Using the relation between $\tau = \sigma - \frac{c}{3b}$, we can insert this into the stationary equation 149 which then only contains the Ginzburg-Landau parameters. One then obtains a cubic equation for α which has a very lengthy, but analytical, solution $\alpha(a)$ for the second-order phase transition line between COE and COE-K^0 phases.The result is illustrated in figure A3.

With the two methods discussed above, we posses analytical expressions for all second order transitions. First

order (critical) lines are determined analytically anyway, which means, that the only region in the entire phase diagram, not determined by an analytical approach is the curved first order line labeled "numerics" in figure (7).

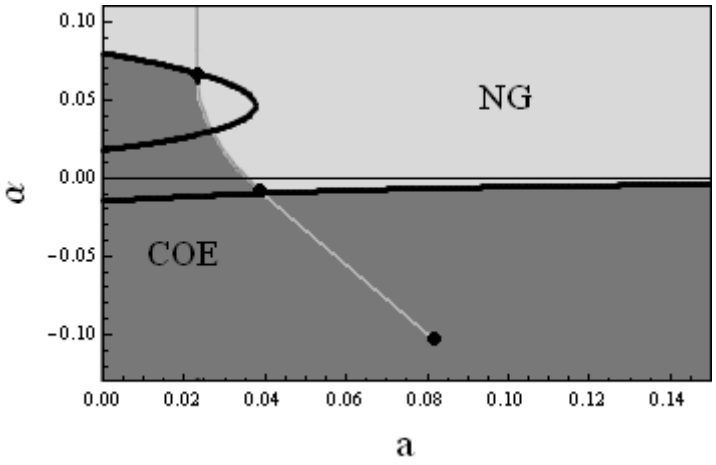

Figure A1: Phase transition-lines, determined by $\alpha = 2\gamma\sigma(a)_{min}$. Since σ_{min} is a solution to a cubic equation, we find different branches which alternating coincide with the (numerical) phase transition-line. All values correspond to figure 11. Not however, that here thick black lines represent the semi-analytically obtained second order transition, whereas first order transition are light gray.

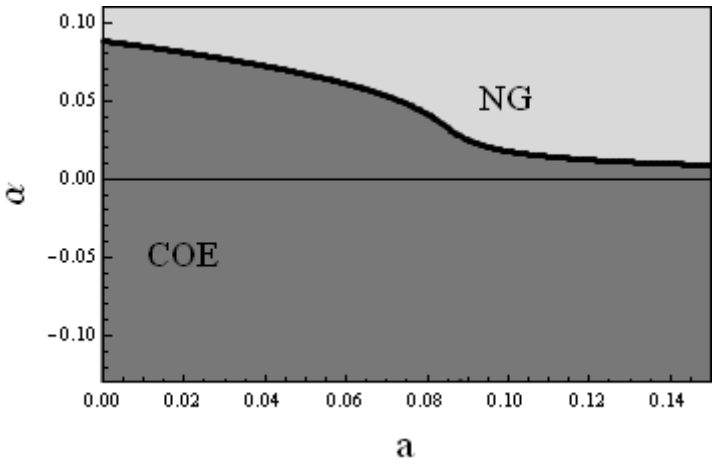

Figure A2: Semi-analytical check corresponding to figure 14.

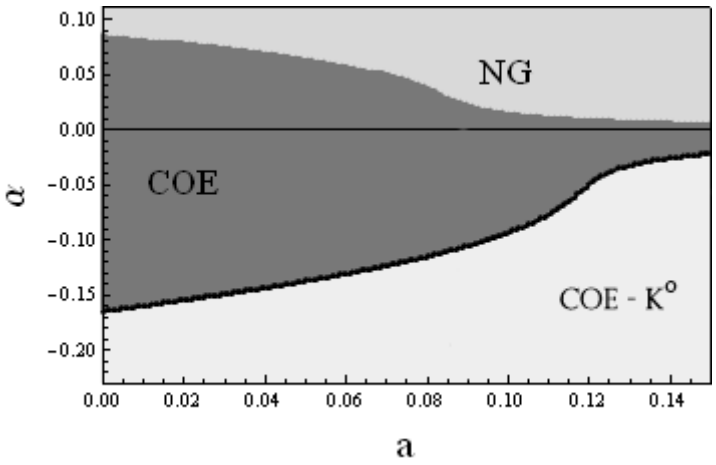

Figure A3: Semi-analytical phase transition-line by using equation 163. Again we have used a thick black line for the semi-analytically obtained second order transition.

References

[1] Walter Greiner, Quantum mechanics - Symmetries, Springer, 1994

[2] G.'t Hooft, Phys. Rev. D 14 (1976) 3432.

[3] G.'t Hooft, Phys. Rep. 142 (1986) 357

[4] D. J. Gross and F. Wilczek, Phys. Rev. Lett. 30, 1343 (1973)

[5] H. D. Politzer, Phys. Rev. Lett. 30, 1346 (1973).

[6] Sidney Coleman, Apsects of symmetries,Cambridge University Press, 1999

[7] Stefan Pokorski, Gauge field theories, Cambridge University Press, 1987

[8] G. Ecker, Chiral perturbation theory, arXiv: hep-ph/9501357v1

[9] Andreas Schmitt, Dense Matter in Compact Stars- A Pedagogical Introduction, ISBN 978-3-642-12865-3

[10] D. T. Son, Phys. Rev. D 59, 094019 (1999),arXiv:hep-ph/9812287.

[11] M. G. Alford, K. Rajagopal, and F. Wilczek, Nucl. Phys. B537, 443 (1999),arXiv: hep-ph/9804403.

[12] M. G. Alford, A. Schmitt, K. Rajagopal, and T. Schafer (2007), arXiv:0709.4635 [hep-ph].

[13] M. G. Alford, A. Schmitt, K. Rajagopal, and T. Schafer (2008), arXiv:0709.4635v2 [hep-ph].

[14] D. T. Son and M. A. Stephanov, Phys. Rev. D61, 074012 (2000), hep-ph/9910491.

[15] D. T. Son and M. A. Stephanov, Erratum Phys. Rev. D 62, 059902(E) (2000)

[16] P. F. Bedaque and T. Sch¨afer, Nucl. Phys. A697, 802 (2002),arXiv: hep-ph/0105150.

[17] M Alford, M Braby, and A. Schmitt, J.Phys.G35:025002,2008, arXiv:nucl-th/0707.2389v2

[18] R. Casalbuoni, R. Gatto, Phys.Lett. B464 (1999) 111-116,arXiv:hep-ph/9908227v2

[19] Tetsuo Hatsuda, Kenji Maeda, Chapter 25 in "Developments in Quantum Phase Transitions" , arXiv:0912.1437v1 [hep-ph]

[20] Dany Page, Sanjay Reddy, Ann.Rev.Nucl.Part.Sci.56:327-374,2006, arXiv:astro-ph/0608360v1

[21] T. Schäfer and F. Wilczek, Phys. Rev. Lett. 82, 3956 (1999), hep-ph/9811473.

[22] M. G. Alford, J. Berges, and K. Rajagopal, Nucl. Phys. B558, 219 (1999), hep-ph/9903502.

[23] Naoki Yamamoto, Motoi Tachibana, Tetsuo Hatsuda, Gordon Baym, Phys.Rev.D76:074001,2007, arXiv:0704.2654v2 [hep-ph]

[24] D. B. Kaplan and S. Reddy, Phys. Rev. D65, 054042 (2002), hep-ph/0107265.

[25] M. G. Alford, M. Braby, and A. Schmitt, J. Phys. G35, 025002 (2008), arXiv:0707.2389 [nucl-th].

[26] M. M. Forbes, Phys. Rev. D72, 094032 (2005), hep-ph/0411001.

[27] H. J. Warringa (2006), hep-ph/0606063.

[28] A. Schmitt, Phys. Rev. D71, 054016 (2005), nucl-th/0412033.

[29] K. Iida and G. Baym, Phys. Rev. D63, 074018 (2001), hep-ph/0011229.

[30] K. Iida and G. Baym, Phys. Rev. D65, 014022 (2002), hep-ph/0108149

[31] K. Iida and G. Baym, Phys. Rev. D66, 014015 (2002), hep-ph/0204124.

[32] Qun Wang, Progress in Physics 30, 173(2010), arXiv:0912.2485v1 [nucl-th]

[33] R. D. Pisarski and F. Wilczek, Phys. Rev. D29, 338 (1984).

[34] D. T. Son (2001), hep-ph/0108260.

[35] M. G. Alford, talk given at workshop "New frontiers in QCD 2010", Kyoto (Japan), http://www2.yukawa.kyotou.ac.jp/ ~ nfqcd10/Slide/Alford.pdf (2010).

[36] M. G. Alford and K. Rajagopal, JHEP 06, 031 (2002), hep-ph/0204001.

[37] S. B. R¨uster, V. Werth, M. Buballa, I. A. Shovkovy, and D. H. Rischke, Phys. Rev. D72, 034004 (2005), hep-ph/0503184.

[38] H. Abuki and T. Kunihiro, Nucl. Phys. A768, 118 (2006), hep-ph/0509172.

[39] H. Abuki, G. Baym, T. Hatsuda, and N. Yamamoto, Phys. Rev. D81, 125010 (2010), 1003.0408.

[40] H. Abuki, G. Baym, T. Hatsuda, and N. Yamamoto (2010), arXiv:1009.3312.

[41] H. Basler and M. Buballa (2010), 1007.5198.

[42] A. Kurkela, P. Romatschke, and A. Vuorinen, Phys. Rev. D81, 105021 (2010), 0912.1856.

[43] F. Ozel, G. Baym, and T. Guver (2010), arXiv:1002.3153.

[44] A. W. Steiner, J. M. Lattimer, and E. F. Brown, Astrophys.J. 722, 33 (2010), arXiv:1005.0811.

[45] A. Kurkela, P. Romatschke, A. Vuorinen, and B. Wu (2010), arXiv:1006.4062.